Volume 54
Number 18
21 September 2025
Pages 8139–8526

Chem Soc Rev

Chemical Society Reviews

rsc.li/chem-soc-rev

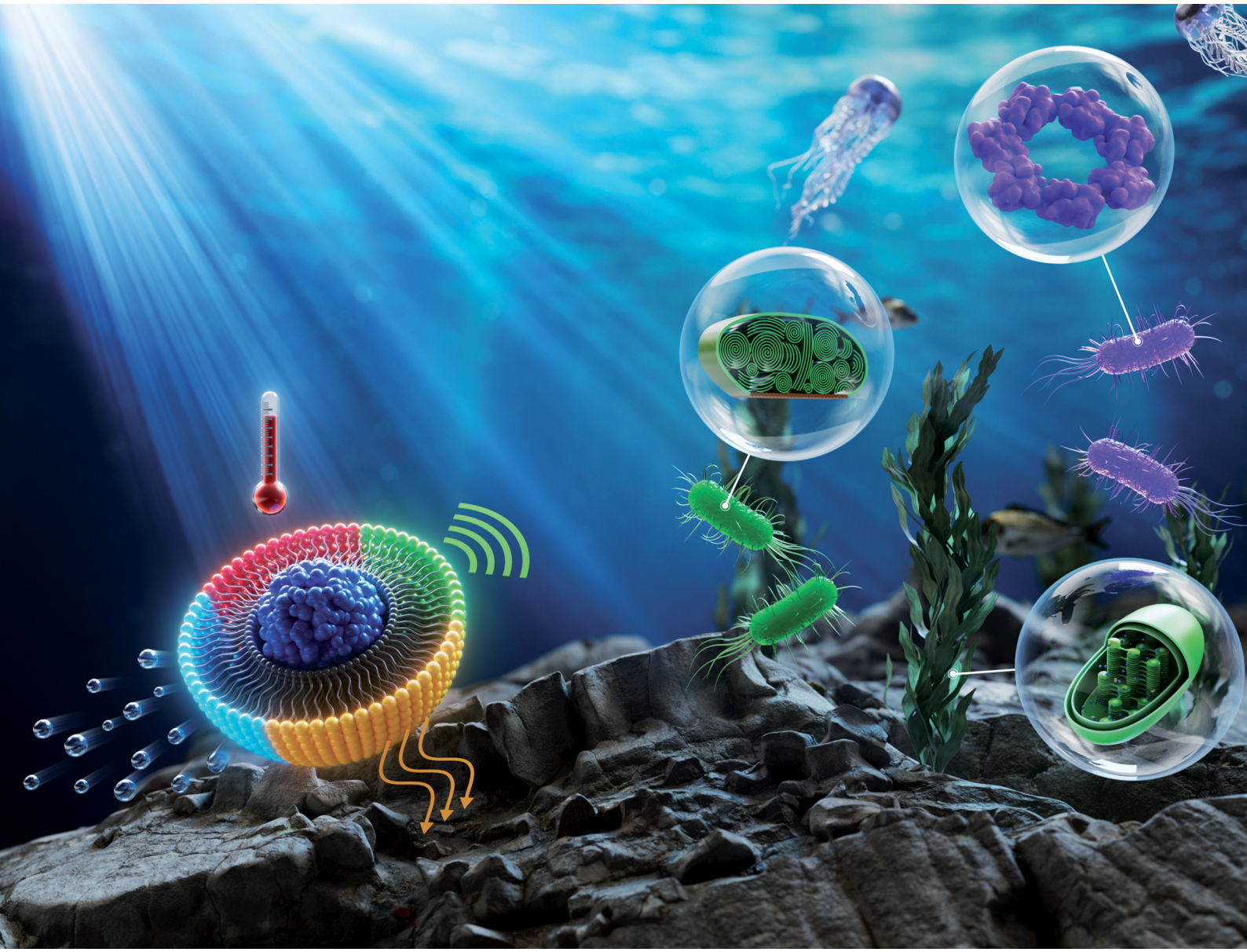

ISSN 0306-0012

ROYAL SOCIETY OF CHEMISTRY

REVIEW ARTICLE
Ali Makky *et al.*
Photoactivatable bioinspired nanomedicines

Chem Soc Rev

REVIEW ARTICLE

View Article Online
View Journal | View Issue

Check for updates

Cite this: *Chem. Soc. Rev.*, 2025, **54**, 8170

Photoactivatable bioinspired nanomedicines

Khatia Merabishvili,[a] Islam Zmerli,[a] Jana Alhoussein,[a] Christophe Regeard[b] and Ali Makky *[a]

Photoactivatable nanomedicines are therapeutic agents that generate heat, produce reactive oxygen species, or initiate photochemical reactions through their interaction with light. These agents can be used for the diagnosis, monitoring and remote induction of therapeutic effects. However, such nanoconstructs may have limitations, primarily attributable to the light–matter interaction and/or to the physiological characteristics of the disease. Consequently, there is growing interest in photoactivatable bioinspired nanoconstructs, which have led to significant improvements in their functionalities. By employing rational design methodologies, biomimicry enables researchers to engineer light-responsive nanomaterials with enhanced functionalities. The bioinspiration from phototrophs, light-harvesting antennas, chlorophylls, and carotenoids has led to the development of unique spatial organizations with broad spectral cross-sections. This resulted in more effective light collection and conversion into chemical energy. For instance, mechanisms like photoprotection can prevent photodamage and ensure treatment safety. In addition, certain animals, particularly marine species, generate or utilize light from other non-photosynthetic species to enhance their function. Finally, photoactivatable nanomedicines bioinspired by the functionalities of DNA scaffolds or biohybridized with cell membranes, cyanobacteria or hemoglobin have been discussed. This review provides a comprehensive perspective on how bioinspiration has contributed to the development of photoactivatable nanomedicines by overcoming some of the conventional nanosystem limitations.

Received 11th March 2025

DOI: 10.1039/d5cs00257e

rsc.li/chem-soc-rev

Open Access Article. Published on 08 July 2025. Downloaded on 1/21/2026 5:41:23 PM.
This article is licensed under a Creative Commons Attribution-NonCommercial 3.0 Unported Licence.

[a] *Université Paris-Saclay, CNRS, Institut Galien Paris-Saclay, Bâtiment Henri Moissan, 17, Avenue des Sciences, 91400, Orsay, France. E-mail: ali.makky@universite-paris-saclay.fr*
[b] *Université Paris-Saclay, CEA, CNRS, Institute for Integrative Biology of the Cell (I2BC), 91198, Gif-sur-Yvette, France*

Khatia Merabishvili

Khatia Merabishvili received her bachelor's degree in chemistry from San Diego State University in 2021. Later, she moved to France to pursue her Master's studies in the Development of Drugs and Health Products at the University Paris-Saclay. She joined the Institute Galien Paris-Saclay in 2023 as an R&D intern. In the same year, she continued as a PhD student to work on smart photoactivatable assemblies to combat local resistant bacterial infections. Her research interests include the synthesis of lipid–porphyrin conjugates, drug delivery systems, and PDT/PTT applications against cancer and resistant bacteria.

Christophe Regeard

Christophe Regeard received his PhD from the University of Rouen in 1999 and, after a postdoctoral fellowship at the EPFL in Switzerland, was appointed Associate Professor of Microbiology at the University of Paris-Saclay in 2004. His career has allowed him to work on a wide range of topics in microbiology, including bacterial genetics, dehalorespiration and environmental biodiversity of bacteria and bacteriophages. Today, his research focuses on the molecular biology of mycobacteria and their phages, as well as on topics at the interface between microbiology and physics (physical properties of biofilms, biocorrosion) and at the interface between microbiology and chemistry (modified surfaces with anti-biofilm properties, antimicrobial nanovectors).

This journal is © The Royal Society of Chemistry 2025

Open Access Article. Published on 08 July 2025. Downloaded on 1/21/2026 5:41:23 PM. This article is licensed under a Creative Commons Attribution-NonCommercial 3.0 Unported Licence.

1. Introduction

Photomedicine is the field of medicine that utilizes light either alone or in combination with light-responsive molecules or nanoconstructs to diagnose, treat, and monitor disease.[1] Although the origin of photomedicine can be traced to ancient times,[2] the science has progressed considerably,[3] particularly with the advent of lasers[4] and its application for the treatment of eye[5] and skin diseases,[6–8] as well as with the discovery of photodynamic[9,10] and photothermal therapies in the 20th century. Subsequent advancements in nanotechnology and photonics have led to the development and application of numerous light-activatable nanoconstructs, utilized for therapeutic and imaging purposes, either *in vitro* or in preclinical studies. The primary applications of light-responsive nanomedicines encompass phototherapy, light-induced drug release, imaging and diagnostics. Upon illumination at a specific wavelength, photoactivatable nanoconstructs transition to an excited state, followed by the emission of the absorbed photonic energy as a fluorescence signal (Fig. 1a). Furthermore, the excited nanomaterials (*i.e.* photosensitizers) can enter the triplet state *via* intersystem crossing where they can transfer their energy to the triplet state of oxygen, leading to the production of singlet oxygen *via* a Type II reaction. Depending on the nature of the photosensitizers and their surroundings, photosensitizers can transfer electrons to the adjacent molecules through a Type I reaction to generate radicals and reactive oxygen species (ROS) that can kill the cancer cells. The efficiency of the photosensitizers in photodynamic therapy (PDT) hinges on the effectiveness of both Type I and Type II reactions. Apart from fluorescence and PDT, the absorbed energy can be dissipated through non-radiative relaxation, resulting in the production of heat that can lead to the destruction of diseased cells and tumor ablation. This process is known as photothermal therapy (PTT) (Fig. 1b). Of particular interest is the phenomenon in which the illumination of photothermal agents with a pulsed laser (nanosecond, picosecond laser) at high irradiance generates ultrasound signals that can be detected by a transducer for imaging purposes. This imaging technique is known as photoacoustic imaging (PAI) (Fig. 1b). Finally, light can be used as a stimulus to trigger the release of a conjugated drug *via* a chemical or physical process in a controlled spatiotemporal manner.[11–13] However, despite these numerous applications, only a few of the developed photoactivatable nanomedicines have been approved for clinical use. This is due not only to technical challenges such as light attenuation in biological tissues caused by the intense light absorption and scattering by the endogenous chromophores (*i.e.* hemoglobin, melanin) and water, but also to systemic challenges ranging from biocompatibility, design complexity, scaling and to the extremely complex physiology of human diseases.[14,15] Consequently, photoactivatable bioinspired nanomedicines have witnessed substantial advancements in recent years, accompanied by numerous pivotal developments aimed at enhancing their biomedical applications.[16]

Biomimicry, encompassing biomimetics and bioinspiration, stands at the core of innovative nanotechnologies that address a range of therapeutic, economic and environmental concerns. Through rational design, biomimicry enables researchers to engineer light-responsive nanomaterials with improved functionalities while preserving or mimicking biological systems or processes. Bioinspiration and biomimetic are two different concepts that include learning nature's design principles and rules to create new models for engineering purposes.[18] Bioinspiration employs a bottom-up strategy and does not always intend to exactly reproduce nature's already developed solutions but instead adapts the primary essences or mechanisms found in nature to solve human or environmental problems. On the other hand, biomimetic is a top-down approach that involves a direct emulation of certain processes found in biological systems.[19] Indeed, nature serves as a perpetual source of inspiration for the design of light-responsive nanomaterials for health applications. For instance, photosynthetic species known as phototrophs exhibit a variety of natural chromophores mainly including chlorophylls and carotenoids. However, they have developed ingenious strategies and unique light-harvesting antennas to efficiently collect light and convert it into chemical energy. This is achieved by tuning the spatial organization of the natural pigment arrays in the light-harvesting systems to obtain a broad spectral cross-section, thereby enabling more efficient light collection under low light-conditions. Furthermore, under conditions of excess light, the photosynthetic systems have evolved mechanisms of photoprotection, allowing them to regulate their light-harvesting capacity and avoid photodamage (Fig. 1c). These natural regulatory mechanisms of light collection and photoprotection have provided a foundation for the development of nature-inspired light-responsive nanomedicines either to enhance their absorption capacity or to protect healthy tissues from photodamage, respectively.[20] Besides phototrophs, light-responsive nanomedicines were inspired by the ability of some marine animals

Ali Makky

Ali Makky has been an Associate Professor of Pharmaceutical Sciences at the University of Paris-Saclay, Faculty of Pharmacy, since 2014. He obtained his Doctor of Pharmacy (Pharm.D.) degree from Saint-Joseph University (Lebanon). He then obtained his Masters and PhD degrees in Pharmaceutical Sciences and Biopharmacy from the University of Paris-Sud. He then joined the SPCSI laboratory at CEA Saclay (France) as a postdoctoral fellow. He then received further postdoctoral training as a Humboldt Fellow in the Laboratory of Physical Chemistry of Biosystems at the University of Heidelberg (Germany). His current research interests focus on the design of organic light-responsive materials for photothermal and photodynamic therapies against cancer and bacterial infections.

Open Access Article. Published on 08 July 2025. Downloaded on 1/21/2026 5:41:23 PM.
This article is licensed under a Creative Commons Attribution-NonCommercial 3.0 Unported Licence.

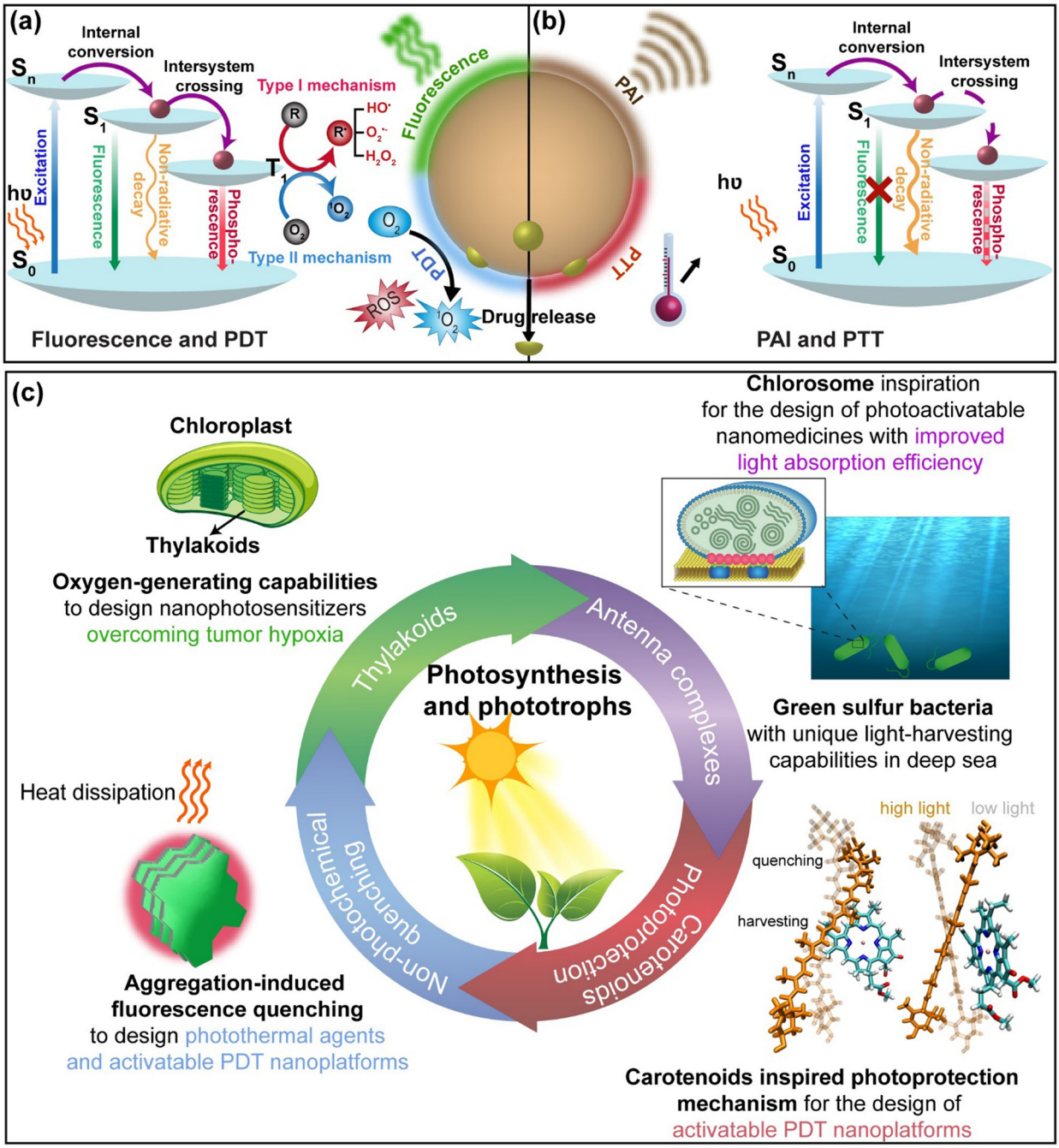

Fig. 1 Schematic representation of light-responsive nanoparticles with multifunctional properties. (a) Simplified Jablonski diagram illustration (b) for the fluorescence/PDT mechanism, and (c) for photoacoustic imaging (PAI) and photothermal process. (c) Schematic illustration summarizing the main inspiration from photosynthesis and photosynthetic systems to design light-responsive nanomedicines. The figure of carotenoids/chlorophyll interaction have been reproduced after permission from ref. 17 copyright 2017 Springer Nature.

to produce light or by other non-photosynthetic species or biological processes to improve their functionality. In consideration of the aforementioned facts, the objective of this review is to report on the various aspects of inspiration from nature or biological systems in the design of advanced light-responsive nanomedicines, with the aim of overcoming the limitations typically encountered with conventional ones. Bioinspired light-responsive nanomedicines can be categorized into two primary classes: The first category includes photoactivatable nanomedicines inspired by photosynthetic systems (*i.e.* green plants and other phototrophs), to enhance their interaction with light and their theranostic outcome. The second category encompasses nanomedicines inspired by marine animals, non-photosynthetic species or biological processes, to improve their physiological and optical performance. This review will provide an overview of how bioinspiration from photosynthesis, phototrophs, and other

This journal is © The Royal Society of Chemistry 2025

Open Access Article. Published on 08 July 2025. Downloaded on 1/21/2026 5:41:23 PM. This article is licensed under a Creative Commons Attribution-NonCommercial 3.0 Unported Licence.

biological structures has advanced the design of photoactivatable nanomedicines, while overcoming the fundamental problems encountered with conventional photomedicines. Additionally, the modification of living photosynthetic cells (*i.e.* cyanobacteria) with artificial materials and photosensitizers, a process known as biohybridization, will be discussed. Finally, the subject of photoactivatable nanomedicines, inspired by the DNA nanostructures and their response to thermal triggers is also described.

2. Photosynthesis-inspired light-responsive nanomedicines

2.1. Inspiration from light-harvesting antennas

The sun is the primary source of energy on Earth. Phototrophs are photosynthetic organisms that contain light-harvesting (LH) antennas carrying out numerous crucial functions in the process of photosynthesis. Theses antennas absorb efficiently the solar energy, enabling not only the migration of excitation energy but also its transfer to the reaction center.[21,22] Therefore, the absorbed photonic energy is converted into chemical energy that is used for biomass production. These antennas are made of several photosynthetic chromophores that can absorb the sunlight efficiently in a wide range of wavelengths.[22,23] These chromophores mainly include chlorophylls, bacteriochlorophylls and carotenoids. Chlorophylls are the primary light absorbers in photosynthesis. To effectively capture light photons and transport excitation energy, they assemble into organized supramolecular structures with the aid of protein or polypeptide scaffolds. This process is exemplified in the case of purple photosynthetic bacteria (Fig. 2a and b).[21] Conversely, other phototrophs such as green sulfur bacteria (Fig. 2c) possess a unique light harvesting complex named chlorosome which enables bacteria to efficiently harvest sunlight and thrive under dim light conditions.[24] Chlorosome is composed of a highly sophisticated arrangement of chlorophyll dyes that do not require the assistance of any protein scaffolds for photon collection (Fig. 2c–g). In fact, the aggregation of hydrophobic chromophores such as porphyrin derivatives or porphyrinoids into well-organized multichromophoric structures enable them to acquire novel photophysical properties compared to their monomeric counterparts. Such phenomena have attracted the attention of many researchers for the development of highly ordered aggregates of chromophores. Two main ordered aggregates of chromophores have been described so far, the H-aggregates and the J-aggregates (Fig. 2h). These two types of aggregates have been categorized by Michael Kasha[25] on the basis of Coulombic coupling as determined by the alignment of the transition dipole moments between two chromophores.[26] Hence, compared to monomers, the aggregates will exhibit energetic shifts in their main absorption peak with subsequent changes in their radiative decay rate. Kasha's model predicts that if transition dipole moments are arranged in a ''side-by-side'' fashion, the resulting aggregates are called H-aggregates and their absorption spectra undergo a blue shift (hypsochromic effect) and a reduction in radiative decay. In J-aggregates, the transition dipole moments are arranged in a ''head-to-tail'' fashion (also called ''edge-to-edge''), which results in a spectral redshift and an increase in the rate of radiative decay. Such intermolecular organization is characterized by their ability to delocalize and migrate excitons.[27] These unique molecular aggregates were discovered by E. E. Jelley[28,29] and G. Scheibe[30] in the 1930s and were referred to later as ''J-aggregates''. However, this classification is not universal for all chromophores where some unconventional aggregates can show a red shift (bathochromic) in absorption spectra but they can exhibit fluorescence quenching.[26,31] The alignment between the monomers depends mainly on their structure which determines the balance between the attractive (π–π stacking, hydrogen bonds and electrostatic attraction) and repulsive forces (steric hindrance and electrostatic repulsion) between the molecules.[32]

2.1.1. Inspiration from photosynthetic purple bacteria for the design of light-responsive nanomedicines with improved light adsorption capabilities in the NIR region. Photosynthetic purple bacteria (Fig. 2a) are anoxygenic photosynthetic species that are widely distributed in aquatic environments and can be classified into two main groups, purple sulfur bacteria and purple non-sulfur bacteria.[36] Compared to purple sulfur bacteria which can poorly grow in the dark, purple non-sulfur ones possess diverse capacities for metabolism and growth in the dark.[36] In addition, and conversely to oxygenic photosynthetic species, which utilize ultraviolet and visible wavelengths for photosynthesis, non-sulfur purple bacteria can absorb light in the NIR region. Light photons in the NIR are efficiently captured by the peripheral antenna (LH2) and the light-harvesting core antenna (LH1) which are then transferred to the reaction center for the photosynthesis. LH2 is composed of two circular organized homomeric aggregates (*i.e.* rings) of bacteriochlorophyll-a pigments named B800 and B850.[37–40] In the B800 ring, the Bchl-a chromophores exhibit weak intermolecular coupling due to the large distance between them (~21 Å) which results in a localized excitation state. Conversely, in the B850 ring, the Bchl-a chromophores are densely packed and exhibit specific edge-to-edge orientation and distance between them, which are maintained by a protein scaffold with a surrounding lipid membrane (Fig. 2b). Such chromophore arrangement enables a shared excitation state among multiple chlorophyll molecules within the ring structure, thus resulting in a significant bathochromic shift in the absorption spectrum of Bchl-a from 800 to 850 nm.[16,33,39,40] Inspired by such pigment arrangements and mainly by the delocalized excitation state in the B850 ring of purple bacteria, Kenneth *et al.*[41] conjugated bacteriopheophorbide-a to 1-palmitoyl-2-hydroxy-*sn-glycero*-3-phosphocholine to obtain bacteriopheophorbide a–lipid conjugates (Fig. 3a and b). These conjugates were formulated at 15 mol% with 5 mol% of DPPE–mPEG$_{2000}$ (1,2-dipalmitoyl-*sn-glycero*-3-phosphoethanolamine-*N*-[methoxy(polyethylene glycol)-2000]) and 80 mol% of DPPC as host phospholipids. The obtained lipid vesicles (referred to as J-aggregated nanoparticles, JNP 16) displayed an enhanced and narrow Q_y absorbance band at 824 nm which corresponds to a 74 nm red-shift when compared to the solubilized monomeric dye (Fig. 3c). The circular dichroism

Open Access Article. Published on 08 July 2025. Downloaded on 1/21/2026 5:41:23 PM.
This article is licensed under a Creative Commons Attribution-NonCommercial 3.0 Unported Licence.

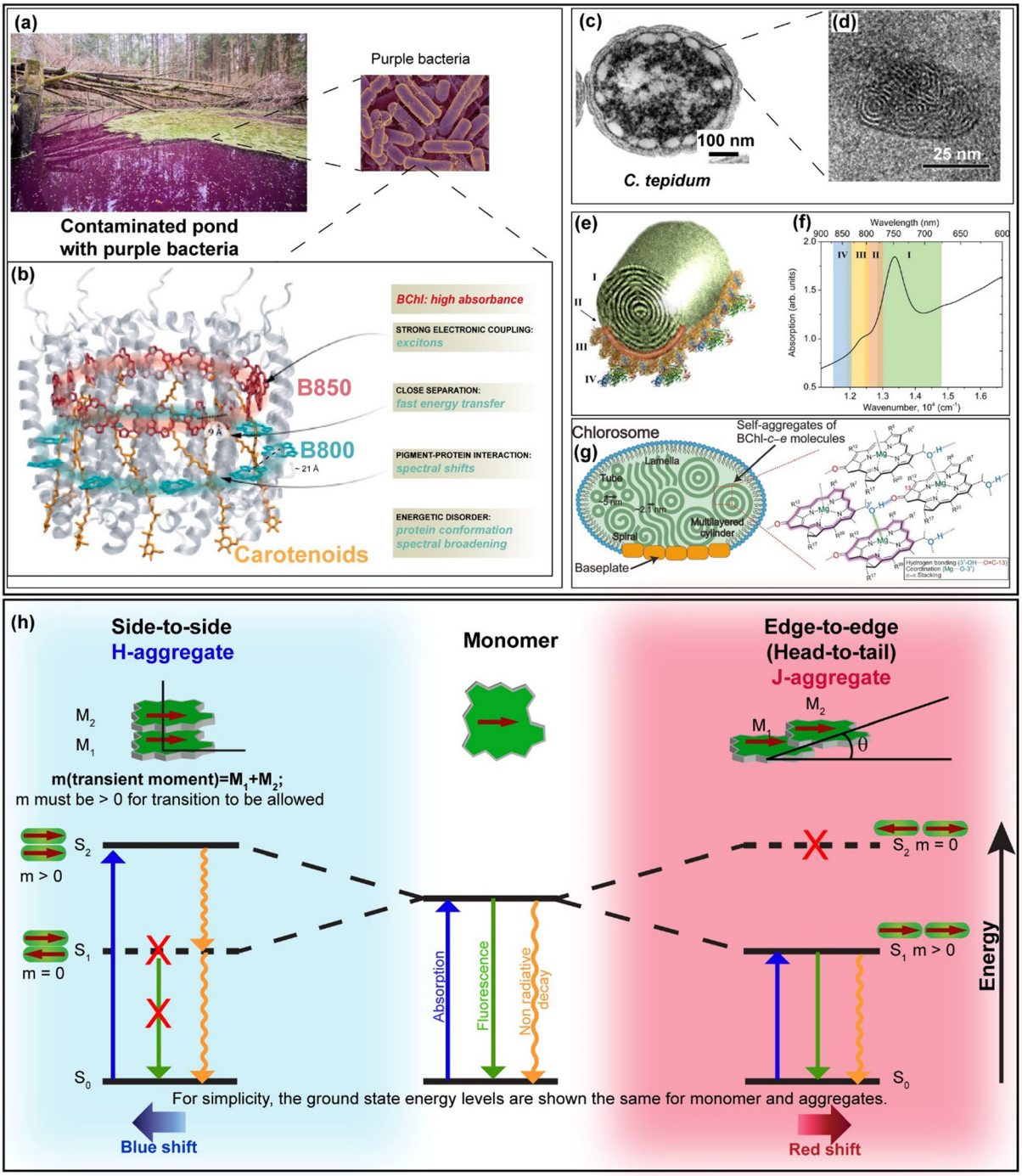

Fig. 2 (a) A photo of a contaminated pond near Hildesheim in Germany (left) with purple bacteria (right). (b) Model of the light-harvesting complex 2 (LH2) found in purple non-sulfur bacteria, illustrating the phenomena that affect the excitation energy transfer.[33] (c) Transmission electron microscopy (TEM) micrograph of a wild type of purple bacteria *Chlorobaculum tepidum* showing chlorosomes as very lightly stained structures surrounding the periphery of the cytoplasm.[34] (d) Cryo-EM micrographs of chlorosomes from wild-type *Chlorobaculum tepidum* fixed in a vertical position in an amorphous ice layer. The micrographs reveal the packing of some lamellae in concentric rings, others in a more irregular association.[24] (e) Scheme representing the structure of the light-harvesting complex (LHC) in green sulfur bacteria highlighting the main components: (I) chlorosome; (II) baseplate; (III) Fenna–Matthews–Olson protein complexes and (IV) reaction centers. (f) Absorption spectrum of a *Chlorobaculum tepidum* bacterial culture showing the Q_y-band. The marked ranges correspond to the different structural units of LHC. The structural unit I is composed of BChl c pigments, while the units II, III and IV contain BChl a pigments.[35] (g) Schematic representation of a chlorosome with the molecular arrangement of the self-aggregated chromophores.[21] (b)–(g) were reprinted and adapted with permission from copyright 2016 American Chemical Society, copyright 2002 American Society for Microbiology, copyright 2010 Springer Nature, copyright 2014 Springer Nature and copyright 2020 Elsevier, respectively. (h) Molecular arrangements of H- and J-aggregates of porphyrinoid derivatives with their corresponding Jablonski diagrams. In the figure, we illustrate the two extreme cases of H- and J-aggregates, where the chromophores either exhibit side-to-side or edge-to-edge arrangement respectively.

 This journal is © The Royal Society of Chemistry 2025

Open Access Article. Published on 08 July 2025. Downloaded on 1/21/2026 5:41:23 PM.
This article is licensed under a Creative Commons Attribution-NonCommercial 3.0 Unported Licence.

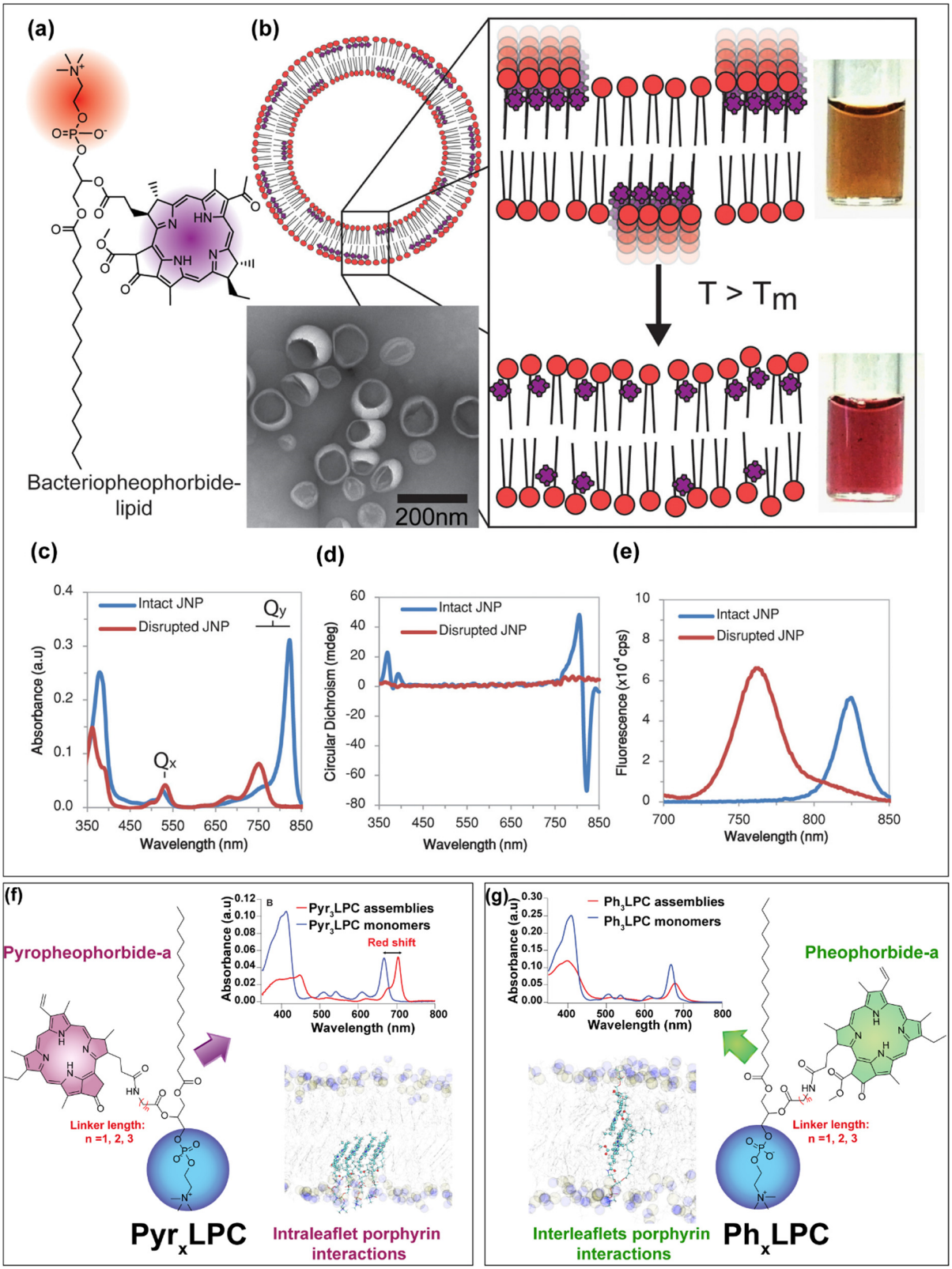

Fig. 3 (a) The chemical structure of bacteriopheophorbide–lipid conjugates which can assemble into (b) J-aggregating nanoparticles abbreviated as JNP (15 mol% Bchl-lipid, 80 mol% DPPC, and 5 mol% DPPE–mPEG$_{2000}$) with colored photographs below and above the phase transition temperature of the host phospholipid. (c) Absorption, (d) circular dichroism and (e) fluorescence spectra of assemblies before (blue) and after (red) their disruption by the addition of detergent. (a)–(e) were reprinted and adapted from ref. 41, Copyright (2014) America Chemical Society. (f) The chemical structure of the Pyr$_x$LPC conjugates with the absorption spectra of the Pyr$_3$LPC assemblies (95 mol% of Pyr$_3$LPC, 5 mol% of DSPE–mPEG$_{2000}$) before (red) and after their disruption with a Triton X-100 detergent. Molecular dynamics simulation snapshot of the Pyr$_x$LPC bilayer showing the preference of intra-leaflet porphyrin interactions. (g) The results correspond to the Ph$_x$LPC conjugates bilayer with their clear preference to form inter-leaflets interaction within the bilayer structure. (f) and (g) were reprinted and adapted with permission from ref. 45, Copyright 2022 The Royal Society of Chemistry.

Open Access Article. Published on 08 July 2025. Downloaded on 1/21/2026 5:41:23 PM. This article is licensed under a Creative Commons Attribution-NonCommercial 3.0 Unported Licence.

spectrum revealed the appearance of a negative effect peak which is related to the formation of ordered chiral packing between the bacteriopheophorbide–lipid molecules (Fig. 3d). In contrast to other lipid porphyrin-conjugates,[42,43] the fluorescence signal of the JNPs was not intensively quenched (Fig. 3e) and exhibited a negligible Stokes shift which provides further evidence the formation of coherently coupled J-aggregates.[41] DPPC (16:0 PC) bilayers disclose a transition temperature (T_m) of ~41 °C. At room temperature or even at the physiological temperature, the DPPC bilayers exhibit an ordered rigid gel phase. However, upon increasing the temperature above the T_m, the bilayer adopts a disordered fluid phase. Such change in the fluidity of the bilayer may influence the packing between the pigments and modify the structure of the J-aggregates. To investigate this hypothesis, the authors prepared different JNPs by using various host phospholipids DMPC (1,2-dimyristoyl-*sn-glycero*-3-phosphocholine; 14:0 PC; T_m ~ 24 °C), DPPC (1,2-dipalmitoyl-*sn-glycero*-3-phosphocholine; 16:0 PC; T_m ~ 41 °C), DHPC (1,2-diheptadecanoyl-*sn-glycero*-3-phosphocholine; 17:0 PC; T_m ~ 50 °C) DSPC (1,2-distearoyl-*sn-glycero*-3-phosphocholine; 18:0 PC; T_m ~ 55 °C) or DNPC (1,2-dinonadecanoyl-*sn-glycero*-3-phosphocholine; 19:0 PC; T_m ~ 62 °C)) which display increasing transition temperature. Interestingly, the authors observed a decrease of J-aggregates absorption at 824 nm upon increasing the temperature above the T_m of host phospholipids with the subsequent appearance of the Q_y band of the monomer at 750 nm. In addition, when the samples were heated above the transition temperatures of the host phospholipids, the photoacoustic signals decreased rapidly. This suggested that the nature of the host phospholipids dictates the ordered arrangement of the pigments inside the bilayer and can be used as thermal sensors for photoacoustic imaging. As proof of principle, the authors succeeded in collecting marked photoacoustic signals at 824 nm after intratumoral injection of JNP16 in KB-tumor bearing mice. At such absorption wavelength, the hemoglobin absorption is low, so the photoacoustic resolution can be improved. Moreover, compared to ICG photoacoustic contrast agent, the photoacoustic signal of JNP16 was sensitive to the temperature upon tumor heating.[41] In another study, the same authors have used the same strategy of embedding bacteriopheophorbide a–lipid conjugates in host phospholipids exhibiting different transition temperatures to develop photothermal enhancing auto-regulated liposomes (PEARLS).[44] Indeed, conventional photothermal agents due to their high absorption at the excited wavelength suffer from high light attenuation which results in reduced depth of heating with large thermal gradients between the superficial and the deeper target tissues. This will provoke collateral damage and inefficient treatment respectively. Hence, taking advantage of the sensitivity of the formed J-aggregates bacteriopheophorbide a–lipid conjugates to the thermoresponsive lipid bilayer, the authors succeeded in designing PEARLs that demonstrate an improved light transmission and regulated photothermal effect with a predefined maximal temperature. This latter can be tuned as a function of the transition temperature of the host phospholipids. When the temperature reaches that of phospholipid transition, the bilayer becomes fluid and the absorption band of the J-aggregates decreases, hence enabling the light to penetrate further.

The proof of principle of PEARLS has been further demonstrated on 3D polyacrylamide hydrogel phantom.[44] In another fundamental study, Charron *et al.*[46] reported that by changing the composition of the lipid bilayer from DSPC to DOPC (1,2-dioleoyl-*sn-glycero*-3-phosphocholine), the bacteriopheophorbide a–lipid conjugates formed disordered aggregates in the unsaturated lipid matrixes. Moreover, despite their fluorescence quenching they maintain significant photodynamic activity, whereas, their incorporation inside a saturated lipid matrix (DSPC), bacteriopheophorbide a–lipid conjugates phase separated inside the saturated lipid matrix and formed highly ordered J-aggregates which offer them very interesting photothermal and photoacoustic properties.[46] Besides, Cui *et al.*[47] have investigated the modulation of organized J-aggregates formation by the lipid scaffold caused Pyropheophorbide-a chromophores incorporation inside DPPC lipid matrix doped with either DOTAP (1,2-dioleoyl-3-trimethylammonium-propane) or DPPG (1,2-dipalmitoyl-*sn-glycero*-3-phospho-(1′-*rac*-glycerol)). The authors[47] found that the electrostatic interaction between the polar headgroup and the carboxyl group of Pyro-a chromophore is the key interaction that governs the ordered J-aggregates. While DOTAP with a positively charged polar headgroup led to a non-organized pattern, the negatively charged headgroup of DPPG showed the opposite tendency. These assemblies were used as specific probes for third harmonic generation microscopy of PC3 living cells and showed significantly enhanced contrast compared to non-ordered aggregates.[47] Following the same line of research, our group has designed several light-responsive nanoconstructs based on the supramolecular assemblies of lipid–porphyrin conjugates.[11,43,45,48,49] They were synthesized by grafting Pheophorbide-a or Pyropheophorbide-a to either lysosphingomyelin[11,43,50] or lysophosphatidylcholine[43,45,48,49] *via* different linker lengths (Fig. 3f and g). The conjugates were able to self-assemble into different supramolecular structures depending on the type of porphyrins. Pheo-a conjugates (Ph_xLPC) assembled into closed ovoid or spongious structures, whereas Pyro-conjugates (Pyr_xLPC) assembled into rigid open sheets. All of the assemblies exhibited intensive fluorescence quenching, with a significant and slight red shift in their Q-band region for Pyr_xLPC and Ph_xLPC respectively. With the aid of molecular dynamics simulations, it was demonstrated that the interaction between the porphyrin moieties rather than the linker length plays a central role in controlling the structure of the assemblies and thus their optical properties.[45,48] While Pheo-a conjugates tend to form interleaflet π-stacked dimers (Fig. 3g), the Pyro-conjugates form dimers within the same leaflet thus hindering the bending of the bilayer (Fig. 3g). Interestingly, all of the conjugates when mixed with equimolar percentage of cholesterol formed liposome-like structures while maintaining intensive fluorescence quenching with a slight red shift in their absorption spectra.[43,45] The formation of liposomal structures was related to the complementarity of the geometrical packing parameters

 This journal is © The Royal Society of Chemistry 2025

Open Access Article. Published on 08 July 2025. Downloaded on 1/21/2026 5:41:23 PM. This article is licensed under a Creative Commons Attribution-NonCommercial 3.0 Unported Licence.

between the conjugates (truncated cone shape) and cholesterol (inverted cone shape).[11,12,45] In addition, our results evidence that the longer the linker, the higher the stability of the assemblies in physiological conditions. This is due to the deeper embedment of the porphyrin core inside the bilayer. Moreover, Pyr$_x$LPC assemblies demonstrated enhanced stability during incubation with serum-containing medium, accompanied by increased photothermal activity and diminished photodynamic activity when compared to Ph$_x$LPC formulations.[49] This result was related to the structural differences in porphyrin moiety, which lead to different packing propensity between the porphyrins inside the assemblies. Moreover, Pyr$_x$LPC conjugates were able to form J-aggregates when incorporated in the lipid bilayer made of phospholipids with high transition temperatures (DPPC, DSPC, DAPC (1,2-diarachidoyl-*sn-glycero*-3-phosphocholine)) which was not the case for Ph$_x$LPC compounds.[45] Hence, by changing the lipid composition of the lipid bilayer, it is possible to tune the formation of J-aggregates and thus their absorption efficiency in the NIR but also their efficacy in the photothermal conversion compared to their photodynamic activity. In comparison to Pyro-a porphyrinoid, Pheo-a has an extra carboxymethyl group in the *ortho* position relative to the ketone functionality which introduces a steric effect hindering the stacking of both sides of porphyrin cores.[45] These conjugates have proven their efficiency in PDT and PTT against cancer cells[43] or bacteria and biofilm[49] but also in light-triggered release of hydrophilic cargo.[11] Recently, our group developed a novel strategy for the design of novel generation of porphysomes, which enables tunable photothermal properties with improved photodynamic efficiency against cancer while maintaining an exceptional high payload of porphyrins (Fig. 4a). The new porphysomes are made of smart PL–Por conjugates, and are composed of one ROS-responsive linker separating the porphyrin moiety from the polar headgroup of the phospholipid (Fig. 4b). Upon their illumination, they enable mild-hyperthermia with subsequent release of the porphyrins moieties, which cause the dissociation of the assemblies (Fig. 4c and d). Moreover, the dissociated lysolipid backbone might act as a detergent-like molecule, which can fragilize the cancer cell membrane thus leading to the enhancement of the therapeutic outcomes. Compared to conventional porphysomes made of Pyrolipid[42] (Pyro-a conjugated to a lysophosphatidylcholine without any linker) or Pyr$_x$LPC (x = 3), the new assemblies demonstrated their versatility and superiority for PDT application *in vitro* (Fig. 4e and f) and *in vivo* against a subcutaneous prostate cancer model. Indeed, the PDT efficiency was improved up to 20-fold *in vitro* and complete tumor ablation was evidenced in 80% of PC3 prostate subcutaneous tumor-bearing mice compared to 0% using conventional porphysomes (Fig. 4g and h).[51]

In addition, the novel porphysomes reduced the dark toxicity of the free porphyrins while maintaining its PDT efficiency.[51] In another example, Wang *et al.*[52] synthesized self-assembled porphyrin photosensitizers for more efficient photodynamic therapy against bacteria. Using zinc *meso*-tetra(4-pyridyl)-porphyrin (ZnTPyP) and CTAB detergent, cubic nanoparticles with an average size of 40 nm were obtained. Nitric oxide was then absorbed into the obtained nanoparticles through the coordination with the central metal Zn ions to form ZnTPyP@NO nanoparticles. These latter improved the photodynamic therapy efficiency due to the subsequent release of ROS and highly reactive peroxynitrite ($ONOO^-$) molecules that exhibited enhanced antibacterial photodynamic activity.

2.1.2. Inspiration from chlorosomes for the design of light-responsive nanomedicines with improved light adsorption capabilities in the NIR region. Compared to other photosynthetic light-harvesting systems, green photosynthetic bacteria such as *Chlorobaculum tepidum*[34] which are anaerobic and thermophilic bacteria, possess another type of light-harvesting antennas called chlorosomes (Fig. 2c–g).[53] These latter are considered as one of the most efficient LH systems enabling green sulfur bacteria that reside at a depth of 100 m under the sea surfaces, to absorb light efficiently under low photon flux conditions. Chlorosomes are characterized by their flattened and ellipsoidal structures with a length of 100–200 nm, width of 30–60 nm and height of 10–20 nm. Also they do not exhibit proteins to maintain the distances and mutual orientations between the pigments.[21] The chlorosome core is the result of the supramolecular assemblies of BChl-c, d, e and f pigments into multilayer tubular or bent lamellar structures.[54–56] BChl orientations are maintained through π–π stacking between the chlorin cores but also through specific hydrogen bonding between the 3^1-hydroxy group and the 13-keto carbonyl moiety and the coordination of the 3^1-hydroxygroup with the central magnesium. The chlorosome core is enveloped with a lipid monolayer embedded with proteins. It has been estimated that each *Chlorobaculum Tepidum* cell contains up to 200 chlorosomes that are composed of 100 000 to 250 000 BChl c molecules per chlorosome. The Bchl molecules assembled within the chlorosomes exhibit J-aggregate characteristics with a large red shift of the Q_y absorption band toward the 700–800 nm wavelength region due to the strong excitonic coupling among the chromophores. Such optoelectronic properties inspired several researchers to design synthetic LH systems mainly for solar cells and artificial photosynthetic devices but also for the design of light-responsive nanomedicines. Such bioinspired nanomedicines enable the improvement of their absorption cross sections, which are crucial for several medical applications such as photoacoustic imaging, fluorescence, photothermal and photodynamic therapies. In this context, Kenneth *et al.*[57] developed ordered J-aggregate structures based on modified chlorin chromophores. These was obtained through the formulation of modified lipid–porphyrin (Lipid–Por) conjugates (20 mol%) in DPPC/DPPE–mPEG$_{2000}$ liposomes (75/5 mol%). To do so, the authors made three modifications on the Pyropheophorbide-a chromophore. First, a methoxy group was inserted into the 3^1 position. Second, the Pyro core was coordinated with a zinc atom. Finally, the modified Pyro-a was conjugated to a lysophosphatidylcholine through esterification. The authors demonstrated that the zinc insertion in the chlorin core enabled axial coordination between the chelated Zn and the 3^1-methoxy-substituent, which was crucial for ordered chlorin aggregation in the lipid bilayer like those observed in chlorosomes.

Open Access Article. Published on 08 July 2025. Downloaded on 1/21/2026 5:41:23 PM.
This article is licensed under a Creative Commons Attribution-NonCommercial 3.0 Unported Licence.

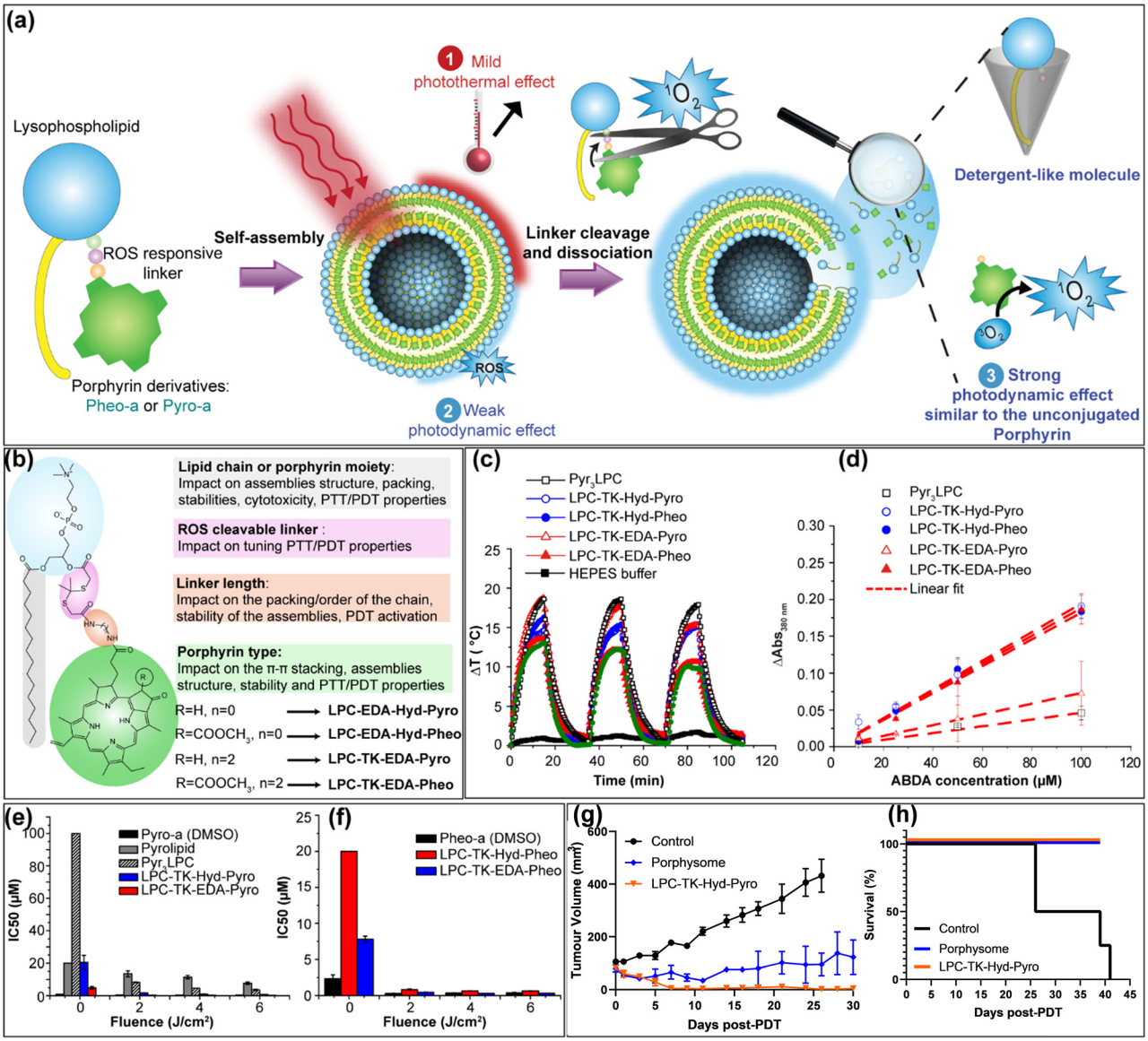

Fig. 4 (a) Schematic representation of the concept of the new porphysomes generation. (b) Scheme representing the structural modifications of the new PL–Por conjugates and their possible impact on the assemblies' properties. (c) The change in temperature (Δ7) (photothermal profiles) of different porphysome formulations at 200 μM of PS concentration under 15 minutes laser illumination (670 nm laser at an irradiance of 0.8 W cm^{-2} at room temperature), followed by a 20 minutes cooling phase (laser turned off). The heating/cooling cycle was repeated three times for each formulation. (d) Normalized absorbance changes (symbols) at 380 nm after 10 min illumination (670 nm, 100 mW cm^{-2}) of the ABDA probe incubated at different concentrations with PL–Por formulations (10 μM of PS) in HEPES buffer indicating the higher photodynamic efficiency of novel porphysomes compared with conventional Py_3LPC. Histograms of IC50 values of (e) Pyro-conjugates and (f) Pheo-conjugates in comparison to the free Pyro-a and Pheo-a in DMSO against PC3 cell lines in the dark (Fluence = 0 J cm^{-2}) and with PDT treatment at different light fluencies (λ = 670 nm, fluence = 2, 4 or 6 J cm^{-2}). (g) Tumor volume (mean ± S.E.M.) measurements up to 30 days post-PDT. (h) Mouse survival monitoring up to 40 days post-PDT. Reprinted and adapted with permission from ref. 51, Copyright 2025 Elsevier.

The obtained vesicles exhibited a hydrodynamic diameter of ~100 nm with an intensive bathochromic shift of 72 nm Q_y band with an increase in the absorbance. These vesicles were then used as a photoacoustic (PA) contrast agent and have proven their efficiency in improving the PA imaging signal on a hamster oral carcinoma model.[57] With the aim to construct more complex and stable chlorosome-like particles without external bilayer template assistance and exhibiting tunable optical properties for photomedicine applications, Harmatys *et al.*[58] used a multi-pronged biomimetic approach by reconstructing chlorosome aggregates into the HDL core–shell biomimetic structure.[20,58] To do so, the authors synthesized first a modified chlorin with a 3^1-OH group and a central zinc metal to replicate the π–π stacking, the hydrogen bonding and the metal–oxygen coordination observed in natural chlorosomes (Fig. 5a). The synthesized chlorin was then conjugated at its 17-position with a lipophilic oleylamine moiety to anchor efficiently these dyes in the lipophilic core of HDL particles using DMPC and R4F as

This journal is © The Royal Society of Chemistry 2025

Open Access Article. Published on 08 July 2025. Downloaded on 1/21/2026 5:41:23 PM.
This article is licensed under a Creative Commons Attribution-NonCommercial 3.0 Unported Licence.

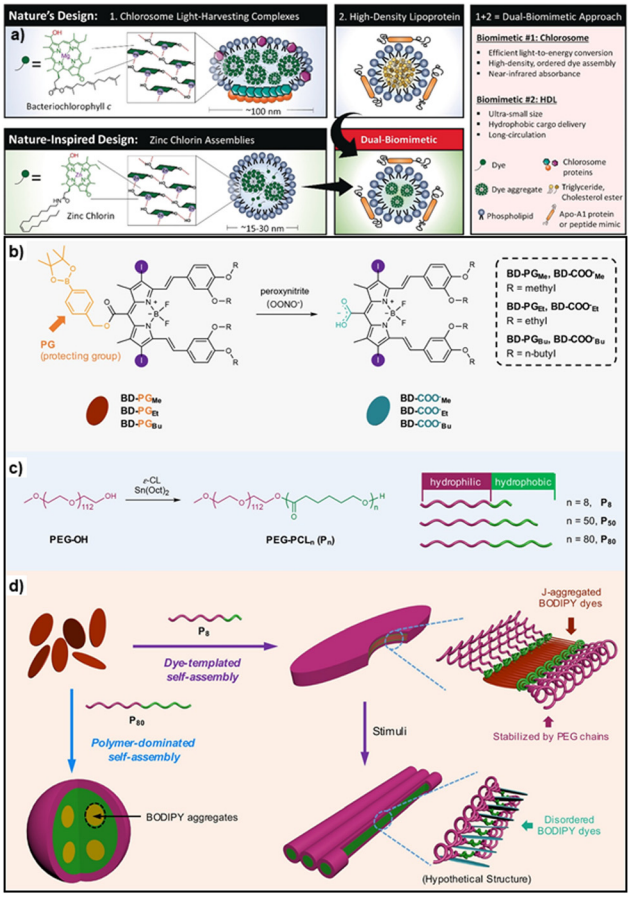

Fig. 5 (a) The strategy adopted by Harmatys *et al.*[20,58] to design bio-inspired chlorosome-like nanoparticles. The design strategy is based on replicating the high-density ordered bacteriochlorophyll dye assembly using a zinc chlorin oleylamide derivative (Chlorin 4) that can self-assemble by noncovalent interactions in the absence of protein assistance, as in chlorosomes. The obtained assemblies were further stabilized within HDL-like nanoparticles to achieve controlled size and structure while maintaining the desired optical properties. Adapted with permission from ref. 58, copyright 2018 Wiley-VCH. (b) Chemical structures of the designed carboxyl-caged BODIPY dyes (BD-PGMe, BD-PGEt, and BD-PGBu), and their stimuli-triggered deprotection chemistry. (c) Synthesis scheme of amphiphilic diblock copolymer PEG–PCL$_n$ (Pn) with different lengths of hydrophobic PCL segments. (d) Schematic representation of the engineered water-stable nanoplates which exhibit a dye slip-stacked arrangement as a core surrounded by a hydrophilic polymeric shell through dye-templated self-assembly. The nanoassemblies when submitted to external stimuli can undergo shape transformation and concomitant rearrangement of dyes from J-stacking to non-stacking arrangement, thus resulting in remarkable optical properties changes. Adapted with permission from ref. 59, Copyright 2018, American Chemical Society.

an external lipid monolayer and Apo-A1 mimetic peptide respectively. The obtained nanoparticles exhibit a spherical shape with a monodisperse distribution with an average diameter of ~11 nm. In addition, the obtained nanoparticles exhibited intensive fluorescence quenching (>90%) and a significant bathochromic shift of 61 nm (from 654 nm to 715 nm) of the Q_y maximum absorption band.[58] The obtained nanoparticles demonstrated their efficiency in their intact form for photoacoustic imaging in the subcutaneous prostate tumor mouse model. In addition, these chlorosome mimicking particles exhibited activatable fluorescence imaging over time following their passive dissociation inside the tumor.[58] Besides porphyrin chromophores, Su *et al.*[59] developed a novel class of BODIPY-based J-aggregates, which are activatable by endogenous peroxynitrite stimuli for selective photodynamic therapy applications while avoiding non-specific photodamage of healthy tissues or skin (Fig. 5b). The developed nanosystem consists of peroxynitrite-responsive iodo-substituted BODIPY dye (BD-PG$_{Me}$) and an amphiphilic diblock copolymer poly(ethylene glycol)-*block*-polycaprolactone (PEG–PCL$_n$) with different PCL segments lengths 8, 50 or 80 denoted as P8, P50 and P80 (Fig. 5b and c). The synthesized BODIPY dye discloses an arylboronate moiety as a protecting group responsive to peroxynitrite to generate *meso*-COOH substituted BODIPY. Copolymers with longer PCL segments (P50 and P80) formed micelles encapsulating the BD-PG$_{Me}$ in the hydrophobic core in both slip-stacked and non-stacked arrangements (Fig. 5d) which appeared under TEM observation as darkened dots with a size of 3–5 nm.[59] In contrast, the P8 polymer possesses weaker self-association properties probably due to a shorter hydrophobic-PCL segment. But it allows the formation of J-aggregated dye-templated nanoassemblies (λ_{max} 788 nm) with a core–shell nanoplate shape (length > 200 nm and thickness around 10 nm) of BD-PG$_{Me}$/P$_8$ as determined by AFM. It should be noticed that other BODIPY dyes with longer hydrophobic chains such as ethyl (BD-PG$_{Et}$) or *n*-butyl chains (BD-PG$_{Bu}$), displayed lower fractions of J-aggregates. The BD-PGMe/P8 nanoplates were remarkably stable in a physiological medium with complete photosensitivity suppression. However, upon their incubation with peroxynitrite at low concentration, the photosensitivity was restored due to the deprotection of the carboxylate group, which disrupted the J-aggregates arrangement. These nanoplates proved to act as specific stimuli-activatable nanophotosensitizers *in vitro* against activated RAW 264.7 macrophages.[59]

2.2. Inspiration from the nature photoprotection mechanisms of the photosynthetic apparatus for the design of safer nanophotosensitizers for PDT applications

Photosynthetic organisms known as phototrophs which include plants, algae and photosynthetic bacteria possess unique and very efficient light-harvesting complexes with unprecedented quantum efficiency, approaching up to 99% of the absorbed photons. These elegant complexes ensure efficient energy transfer to the reaction centers of the photosynthetic units.[60,61] In addition, light-harvesting systems have a dynamic nature and can self-regulate their light absorption properties to operate both under dim light and intense sunlight conditions. Indeed, intense sunlight can provoke photodamage due to the generation of reactive oxygen species (ROS). Hence to avoid any possible photodamage, plants have developed several photoprotective mechanisms mainly (i) by quenching the excited state of chlorophylls under excessive excitation through non-photochemical quenching (NPQ) or (ii) through rapid transfer of electrons to acceptors within the chloroplast such as carotenoids.[60] NPQ is the most efficient mechanism, which dissipates the excessive light excitation into heat before it can be

Open Access Article. Published on 08 July 2025. Downloaded on 1/21/2026 5:41:23 PM. This article is licensed under a Creative Commons Attribution-NonCommercial 3.0 Unported Licence.

transferred to the photosynthetic reaction centers. NPQ is characterized by a strongly reduced chlorophyll fluorescence lifetime caused by the clustering of light-harvesting antenna and/or by the energetic interconnectivity between them.[60] This kind of photoprotecting mechanism has prompted the development of light-responsive nanoconstructs to enable not only activatable photodynamic therapy but also photothermal therapy and photoacoustic imaging. For instance, chlorophyll or porphyrin derivatives have been conjugated to lipid derivatives,[42,43,62] peptides[63] or polymers[64] to design amphiphilic conjugates, which can self-assemble into supramolecular structures[65] with a high density of porphyrins within the assembly. Such assemblies exhibit high fluorescence quenching due to the intensive π–π stacking between the porphyrin moieties, thus upon the illumination, the absorbed photonic energy will be mostly dissipated into heat with a drastically low yield of singlet oxygen generation and fluorescence. However, upon their internalization inside the targeted cells, they will dissociate by releasing the monomeric conjugates which in turn recover their fluorescence and their photodynamic activity.[66] Besides the NPQ mechanism, carotenoids are essential pigments in both photosynthesis and in protecting photosynthetic organisms from photodamage.[67–69] Indeed, compared to chlorophylls, carotenoids can absorb light strongly in the blue-green region (450–550 nm) and transfer the excitation energy to chlorophylls. This enables the expansion of wavelength light range of absorption to efficiently drive the photosynthesis. In addition, carotenoids can protect the reaction centers of photosynthetic organisms from the excess light exposure *via* the triplet–triplet energy transfer from chlorophylls to them.[67] Inspired by the photoprotection mechanism of carotenoids, Moore *et al.*[70] investigated the structural requirements needed for carotenoid photoprotection, by synthesizing different carotenoid–porphyrin dyads.[70] By formulating one of these dyads either in liposomes or in emulsion, the authors demonstrated specific accumulation of the carotenoporphyrins in the tumor in mice bearing the MS-2 fibrosarcoma model. This conjugate enables selective tumor imaging while avoiding singlet oxygen generation and photodamage of healthy tissues. Indeed, in caroteno–porphyrin dyads, the carotenoid completely suppresses the formation of singlet oxygen, but has little effect on the porphyrin singlet-state properties, including fluorescence.[70] Similarly, Chen *et al.*[71] designed an enzyme-responsive Pyropheophorbide–peptide–carotenoid (PPC) conjugate, which was synthesized by linking the two molecules *via* a cleavable caspase-3 substrate (GDEVDGSGK). In comparison to free Pyropheophorbide–peptide, PPC exhibited 8-fold less $^1O_2$. The incubation of caspase-3 with PPC resulted in a 4-fold increase in $^1O_2$ signal, thus indicating the high efficiency of the carotenoid in quenching the singlet oxygen production.[71] Although promising, this kind of strategy may present limited PDT potency toward the cancer cells since the cleaved carotenoids can interact with the released photosensitizers and quench the singlet oxygen generation.[20]

2.3. Bioinspiration from thylakoids for the design of photoactivatable nanomedicines overcoming tumor hypoxia hurdles

Photosynthesis occurs within abundant vegetable cellular organelles called chloroplasts and more precisely, in a network of membranes known as thylakoids (Fig. 1c).[72] Chloroplasts are characterized by three main compartments: (i) the envelope which consists of a double membrane that delimits the chloroplast itself; (ii) the stroma which corresponds to an aqueous phase mainly composed of soluble proteins, and (iii) an internal membrane system, the thylakoids, which contains the major photosynthetic protein complexes (photosystem II (PSII), cytochrome b6f (cytb6f), photosystem I (PSI), and ATP synthase). The PSII photosystem complex is responsible for the light-driven O_2 production in plants, algae or cyanobacteria where a molecule of O_2 is generated from two water molecules in four light-driven electron-transfer steps. This process involves several redox species and starts with the photoexcitation of a chlorophyll special pair called P680 followed by a primary charge transfer between the electron donor and acceptor sides of PSII.[72] However, to avoid oxidative damage in plants, they developed robust antioxidant systems in both the stroma and the thylakoid membranes. For instance, catalase enzyme embedded in the thylakoid membrane can efficiently decompose toxic H_2O_2 into O_2.[73,74] Inspired by the unique functions of thylakoids, Ouyang *et al.*[75] prepared nanothylakoid (NT) particles to overcome tumor hypoxia by decomposing tumor endogenous H_2O_2 into O_2 (Fig. 6). Indeed, added to the hypoxic environment of solid tumor, PDT can further exacerbate tumor hypoxia due to the fast O_2 consumption during the treatment. This will in turn reduce the PDT efficiency.

The NTs were prepared from chloroplasts, which were isolated from spinach leaves (Fig. 6). The nanothylakoids were then obtained from the thylakoid membranes through extrusion. The obtained NTs exhibited a nanovesicle structure with a hydrodynamic diameter of ∼50 nm and a membrane thickness of ∼9 nm. The researchers demonstrated the capacity of the NTs to produce singlet oxygen in a highly efficient manner under conditions of both normoxia and hypoxia. This capability is attributable to the NTs hypoxia modulation activity, which is facilitated by catalase enzyme. Interestingly, the NTs have proven their photodynamic efficiency *in vitro* against 4T1 cancer cells and *in vivo* against the subcutaneous tumor-bearing mouse model. The thylakoid-inspired drug delivery systems for biomedical applications have been recently reviewed and published by Kong *et al.*[76]

2.4. Nature-inspired multichromophore complexes for the design of photoactivatable nanomedicines with enhanced fluorescence properties

Fluorescence bioimaging with a high signal-to-background ratio (SBR) and high selectivity toward the diseased tissue is considered an efficient imaging approach for theranostics as well as in surgery fluorescence-guided imaging. Although interesting, fluorescence imaging suffers from some key issues which include low penetration depth of light especially for chromophores absorbing in the visible (400–700 nm) NIR-I region (700–900 nm), light scattering, autofluorescence, quenching and photobleaching.[14] To improve the light penetration depth and to increase the SBR, several researchers have already designed chromophores that can absorb light in the NIR-IIa (1300–1400 nm) and NIR-IIb (1500–1700 nm) with

 This journal is © The Royal Society of Chemistry 2025

Open Access Article. Published on 08 July 2025. Downloaded on 1/21/2026 5:41:23 PM.
This article is licensed under a Creative Commons Attribution-NonCommercial 3.0 Unported Licence.

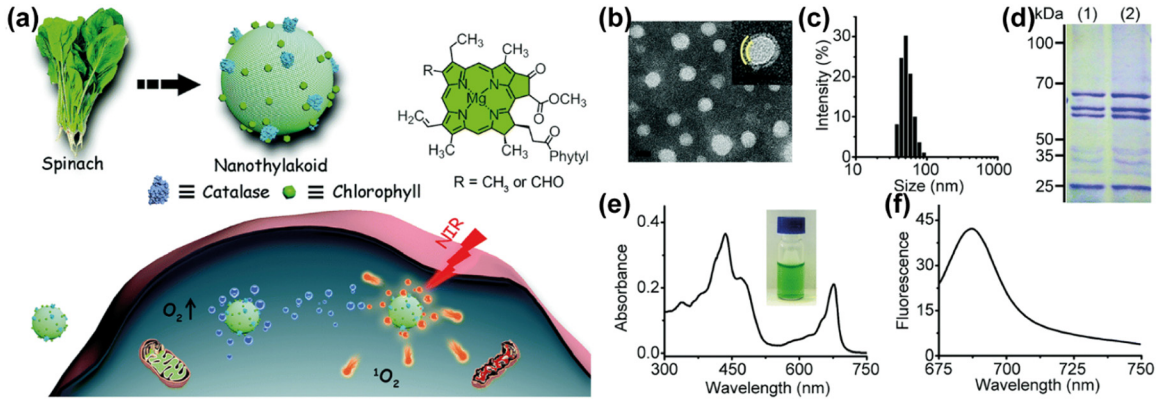

Fig. 6 (a) Schematic representation of the preparation of the nanothylakoids containing chlorophyll, catalase, and their utilization as efficient nanocarriers for PDT applications against cancer. (b) Negatively stained transmission electron microscope (TEM) micrographs of nanothylakoids. (c) Dynamic light scattering size distribution analysis of the nanothylakoids. (d) Membrane protein analysis by SDS-PAGE revealing that the (1) thylakoid membrane and (2) nanothylakoids preserved most of the membrane proteins. (e) UV-Vis absorption spectrum of the nanothylakoid suspension with their photo in the inset. (f) Fluorescence spectrum of the prepared nanothylakoids. Adapted and reprinted with permission from ref. 75 Copyright 2018, RSC Royal Society of Chemistry.

improved fluorescence intensity.[14] Besides the synthesis of new fluorescent probes, the lessons learned from the J-aggregation in multichromophore complexes have inspired researchers to develop photoactivatable nanoconstructs with enhanced fluorescence properties for biomedical applications. In fact, the restriction of intramolecular motions of the chromophores with subsequent improvement in the fluorescence can be obtained by inducing organized aggregation such as the formation of J-aggregates. The formation of J-aggregates is not solely interesting for improving the absorption of chromophores by shifting their absorption bands to longer wavelengths but also for the design of nanoconstructs with enhanced fluorescence in the NIR. In particular, the aggregation-induced emission (AIE) in the NIR-II represents a unique strategy for enhanced fluorescence resolution for clinical applications. In AIE, the chromophores only fluoresce upon their aggregation in specific conditions such as high concentration, solvent polarity, enzymatic reaction, *etc*. In addition, in the NIR-II range, the light exhibits deeper tissue penetration than shorter wavelengths; the tissues have very low autofluorescence signals (Fig. 7a and b) thus selective and highly resolved fluorescence can be obtained.[77] Although interesting, J-aggregates usually encounter a major problem of instability under physiological conditions due to their dissociation in the presence of blood proteins, lipoproteins or cells, which limit their utilization in biomedical applications (Fig. 7c). Consequently, various methods have been described for the stabilization of such aggregates for *in vivo* applications including the use of lipidic or polymeric drug delivery systems or the structure chemical modification to tune the formation of stable J-aggregate chromophores under physiological stimuli. Whereas the formation of J-aggregates in chromophore delivery systems is dependent on the carrier structure and leads to fragile aggregates, the chemical modification of the chromophores enables the design of activatable and stable aggregates under physiological conditions. Consequently, Li *et al.*[78] designed a series of solid-state fluorophores based on 2-(2-hydroxyphenyl)-4(3*H*)-quinazolinone (HPQ) derivatives to obtain stable J-aggregates *in vivo* which fluoresce in the NIR-II region (1000–1200 nm) with low or anti diffusion properties allowing selective imaging of the tumor as well as its precise resection. This wavelength range enables high fluorescence resolution due to the higher penetration depth and the low auto-fluorescence of endogenous pigments. HPQs are classical and well-known chromophores for AIE applications. Such chromophores can interact together *via* strong intra and intermolecular H-bonding interactions to form highly fluorescent aggregates. Thus, they can be used as active fluorescent probes at a given site upon their selective aggregation (Fig. 7c and d). Among several HPQ derivatives designed by Li *et al.*,[78] HPQ-Zzh-B appeared to be the most successful compound for *in vivo* fluorescence imaging. This compound consists in fusing a HPQ unit onto the conjugated structure of a simple hemi-cyanine dye and protecting the hydroxyl group with phenylboronic acid pinacol ester, which is an $ONOO^-$ sensitive group. HPQ-Zzh-B was not fluorescent under physiological conditions. However, upon removal of the protecting group by $ONOO^-$ ions, which are present at high concentration in tumors, the released dye molecules were able to form J-aggregates *in situ* with strong NIR-II fluorescence. Interestingly, these aggregates exhibited very low diffusion and maintained stable and selective fluorescence inside the tumor even after 8 hours following their intratumoral injection in 4T1 subcutaneous tumor-bearing mice. Finally, the authors demonstrated the efficiency of such *in situ* formed aggregates for fluorescence image-guided cancer surgery in mice.[78]

3. Bioinspiration from non-photosynthetic species for the design of light-responsive nanomedicines

3.1. Inspiration from marine animals for the design of photoactivatable nanoconstructs with improved fluorescence properties or other functionalities

The discovery of fluorescent proteins in marine animals including green fluorescent protein (GFP) found in jellyfish, has

Open Access Article. Published on 08 July 2025. Downloaded on 1/21/2026 5:41:23 PM.
This article is licensed under a Creative Commons Attribution-NonCommercial 3.0 Unported Licence.

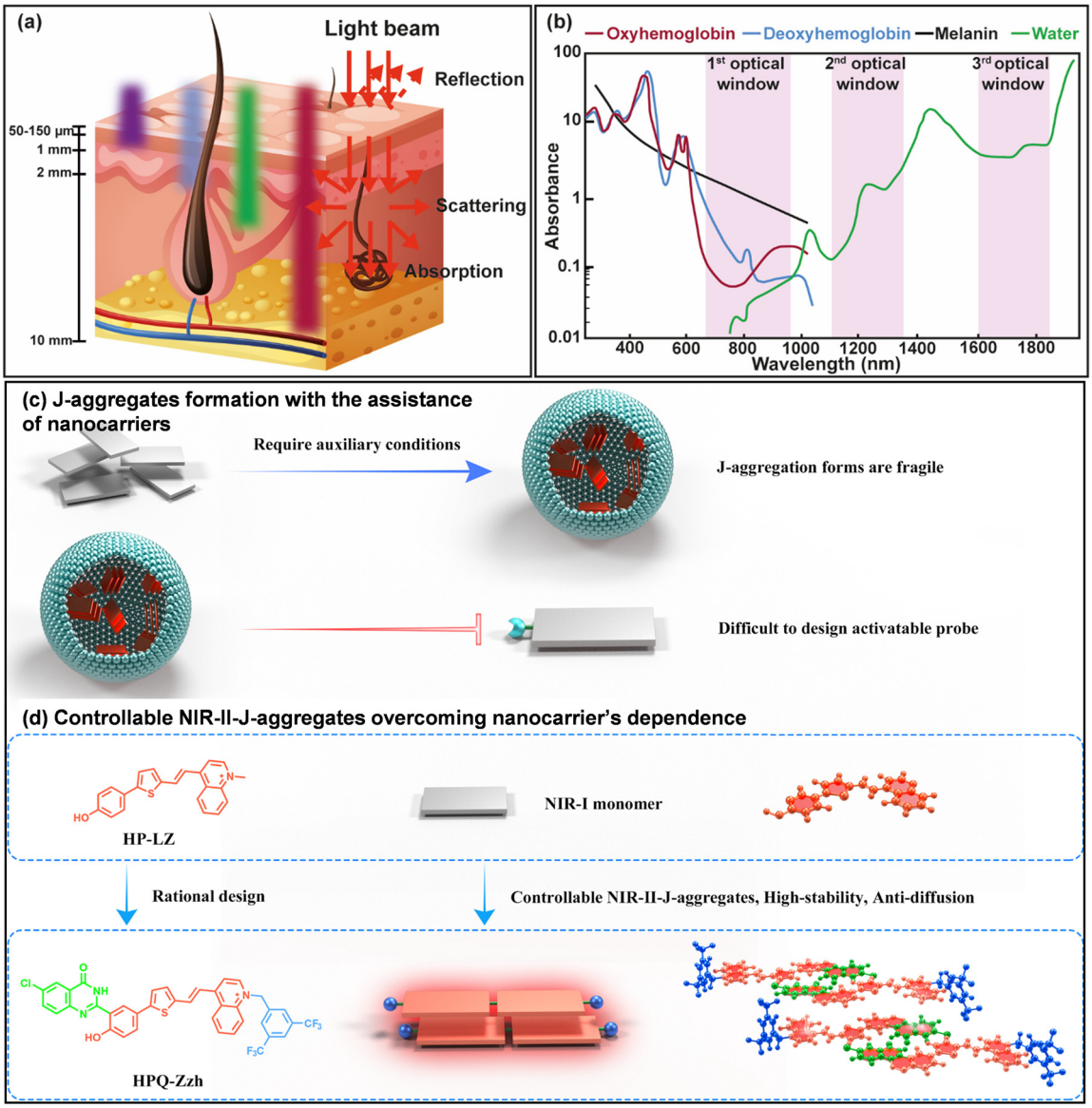

Fig. 7 (a) Scheme of skin illustrating the light penetration depth as a function of wavelength. (b) Absorption spectra of tissue chromophores and water. Note the presence of three optical therapeutic windows, where the absorption of endogenous pigments and water is minimal for maximal light penetration. (c) Schematic representation of the conventional J-aggregation chromophore preparation method, which requires the use of nanocarriers to assist stabilization. (d) The novel approach adopted by Li *et al.*[78] for the formation of stable NIR-II-J-aggregates without the need of nanocarriers. The red part represents the HP-LZ chromophore, the green part represents the HPQ unit, and the blue part represents the hydrophobic groups. Adapted with permission from ref. 78, Copyright 2023, Nature Publishing Group.

prompted researchers to mimic such fluorescence behavior. GFPs from the jellyfish *Aequorea Victoria* have been extensively utilized as fluorescent probes to monitor gene expression, protein localization and for numerous other biological studies.[79] The interesting fluorescence properties of GFPs are related to the location of the fluorescence chromophore *p*-hydroxybenzylidene-2,3-dimethylimidazolinone (*p*-HOBDI) at the center of a β-sheet barrel which shields them from the external quenchers while offering steric hindrance which disables the free rotation of the aryl substituents and the formation of a hydrogen-bond network that prevents the cis/trans isomerization pathway (Fig. 8a).[79,80] Such chromophore conformation suppresses the non-radiative relaxation and facilitates excited state proton transfer. The GFP chromophore is formed *via* autocatalytic oxidized dehydration of a tripeptide motif (Ser-Tyr-Gly) with subsequent cyclization of the chromophore.[81] Mimicking the steric hindrance of the GFP cavity enabled researchers to develop a GFP chromophore analogous with the restricted rotation of the aryl–alkene bond, thus leading to improvements in their fluorescence intensities and quantum yields. Besides the chemical modification of the GFP chromophore skeleton, their incorporation into nanoscale cavities[82,83] such as metal–organic frameworks (MOFs) allow the chromophores confinement while maintaining their rigid

 This journal is © The Royal Society of Chemistry 2025

Open Access Article. Published on 08 July 2025. Downloaded on 1/21/2026 5:41:23 PM.
This article is licensed under a Creative Commons Attribution-NonCommercial 3.0 Unported Licence.

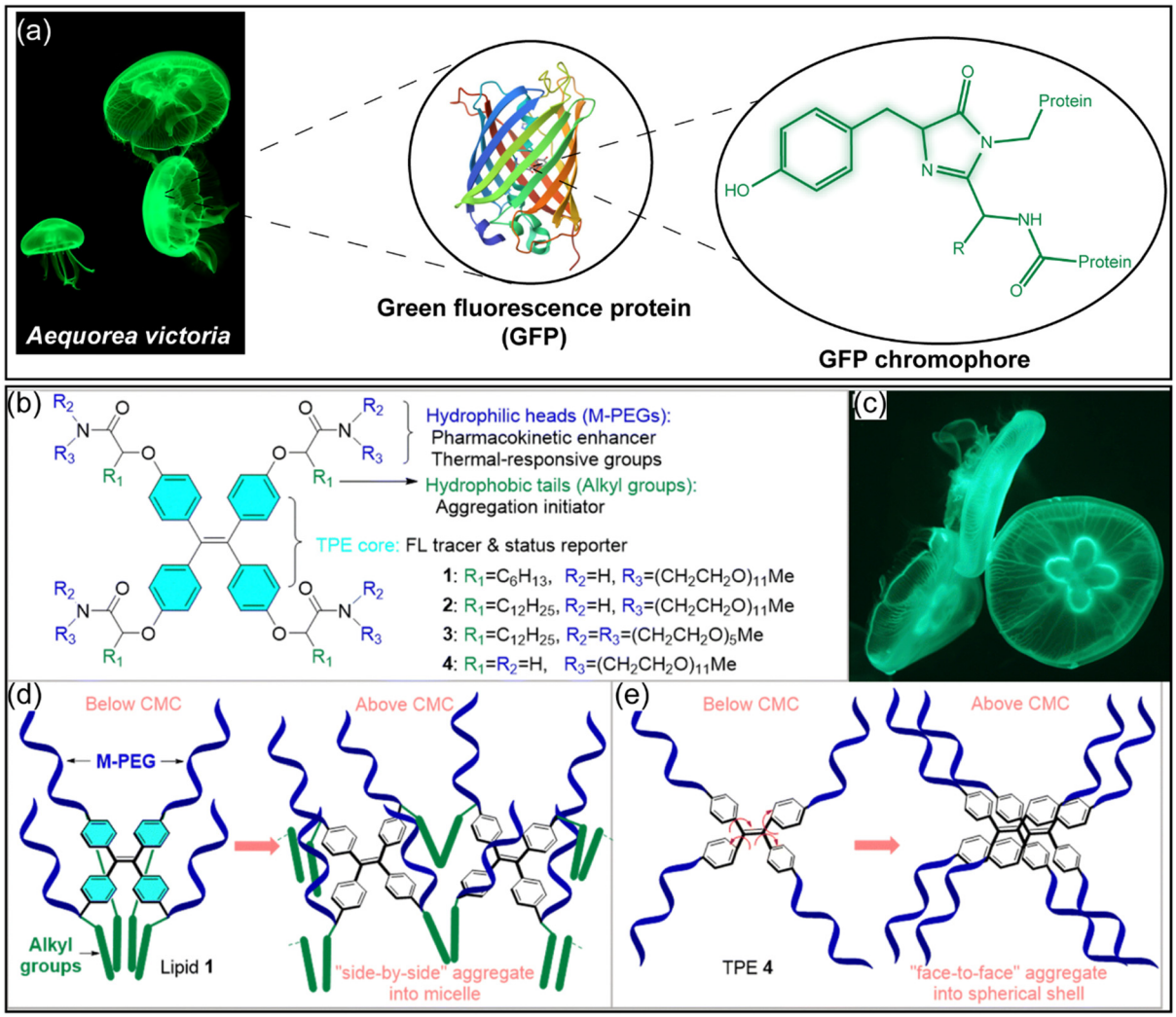

Fig. 8 (a) Crystal structure of GFP (GFP/S205V mutant, Protein Database (PDB) entry 2QLE) from *Aequorea victoria* showing the GFP chromophore immobilized inside the barrel. (b) Chemical structures of TPE lipids 1–3 and hydrophilic TPE 4 inspired by (c) the glowing shape of the jellyfish. (d) The proposed mode of aggregation of lipids–TPE 1–3 and (e) lipid–TPE-4. (b)–(e) were adapted and reprinted with permission from ref. 85, Copyright 2023, The Royal Society of Chemistry.

molecular conformation. A review about this aspect has been recently published.[84] In addition to the GFP conformation and the fluorescence yield enhancement, Zheng *et al.*[85] were inspired by the glowing structure of the moon jellyfish to design smart fluorescent lipids consisting of tetrasubstituted tetraphenylethene (TPE) with four symmetrical amphiphilic side chains composed of m-PEG and alkyl chains (Fig. 8b–e). The m-PEG and the alkyl chains (either *n*-dodecyl or *n*-hexyl group) resemble the bell and tentacles of the moon jellyfish,[85] whereas the TPE core can be assimilated to the glowing 4-blade core. The balance between the pegylation and alkylation controlled the aggregation of these compounds and thus their AIE, fluorescence yield, stability, cell internalization and toxicity. The authors showed that below the critical micelle concentration (CMC), the amphiphilic compounds 1–3 facilitated the intramolecular interaction between the alkyl chains while maintaining the TPE core at the hydrophilic–hydrophobic interface, which restricted its intramolecular movement. Interestingly, above the CMC the compounds 1–3 formed spherical nanoparticles with a ''side-by-side'' aggregation and AIE which was promoted by the steric hindrance offered by either the m-PEG chains or the hydrophobic alkyl groups in comparison to the compound TPE-4.[85]

Another example of inspiration from marine animals is the developed vision system of some deep-sea fishes known as dragon fishes.[86] These later possess chlorophyll antenna in the proximity of opsin-bound retinal complexes.[87] This antenna can efficiently absorb red light under deep-sea conditions, with a subsequent triplet-energy transfer mechanism to the nearby retinal molecules, which undergo photoisomerization from *cis*-retinal to *trans*-retinal conformation. This photoisomerization facilitates a change in the conformation of the opsin protein, thereby enabling the fish to detect the red light.[87] Similar to retinal, azobenzenes are a class of molecules widely employed

Open Access Article. Published on 08 July 2025. Downloaded on 1/21/2026 5:41:23 PM.
This article is licensed under a Creative Commons Attribution-NonCommercial 3.0 Unported Licence.

in numerous applications as photoswitches due to their capacity to undergo photoisomerization from their stable *E* isomer to the *Z* metastable one.[88] However, such photoswitchable reactions generally necessitate the utilization of short wavelengths in the UV region, a limitation that restricts their application, particularly under *in vivo* conditions. Inspired by the visual system of deep-sea fish, Gemen *et al.* adopted the disequilibrium by sensitization under the confinement (DESC) approach. The latter involves the selective caging of the stable *E*-isomer azobenzene with a dye (BODIPY, resazurin, resorufin), which acts as an antenna. The components of the supramolecular system used for DESC consist of six Pd^{2+} ions and four triimidazole ligands, as well as a photosensitizer that were assembled together. Upon illumination at different wavelengths, including red, the photosensitizer undergoes a transition from the ground state to the singlet-excited state. However, the confinement offered by the cage promotes the intersystem crossing of the dye to its triplet state. The azobenzene dynamics facilitates the dye to azobenzene triplet-energy transfer, thereby enabling the azobenzene to adopt its *Z* isomer.[87] This strategy offers a promising avenue for the utilization of azobenzene photoswitches in numerous applications.

3.2. Bio-inspiration from marine species for the design of self-illuminated PDT nanomaterials or adhesive photoactivatable delivery systems

Bioluminescence is a chemical process that enables certain living species, including some insects and marine organisms to produce visible light. In the deep sea, some species of fish, such as anglerfish display a dangling lure (*i.e.*, "esca") on the top of their heads (Fig. 9a).[89] This organ serves as a habitat for symbiotic bacteria identified as *Photobacterium phosphoreum* which can generate light through a bioluminescent reaction.[90] Bacterial luciferase is a two-component flavin-dependent monooxygenase that binds to reduced flavin mononucleotide ($FMNH_2$, $FMNH^-$) and catalyzes its oxidation in the presence of molecular oxygen to form a C4a-peroxyflavin intermediate (Lux:$FMNHOO^-$). This intermediate undergoes further reactions after its reaction with the aldehyde substrate to form the luminescent emitter (C4a-hydroxyflavin, Lux:FMNHOH), emitting blue-green light (Fig. 9b).[91] The bioluminescence mechanism has inspired researchers to develop self-illuminated PDT nanoplatforms to overcome the limited penetration depth of external light for their activation.[92,93] Indeed, the engineering of self-illuminated nanoplatforms can be accomplished through the implementation of either bioluminescent resonance energy transfer (BRET) or chemiluminescent resonance energy transfer (CRET), thereby enabling the photoactivation of the PS without the necessity of an external light source.[93,94] The distinguishing characteristic between these two processes lies in the origin of the substrates involved in the luminescence mechanism. In particular, BRET is based on the transfer of energy from a bioluminescent donor to an acceptor in the presence of an enzyme, with luciferase being a well-known example of a bioluminescent enzyme. Conversely, CRET involves a FRET mechanism subsequent to a chemical reaction catalyzed by an endogenous stimulus, such as hydrogen peroxide found in cancer cells or a chemical compound like luminol. The processes are outlined in more detail in Fig. 9c.

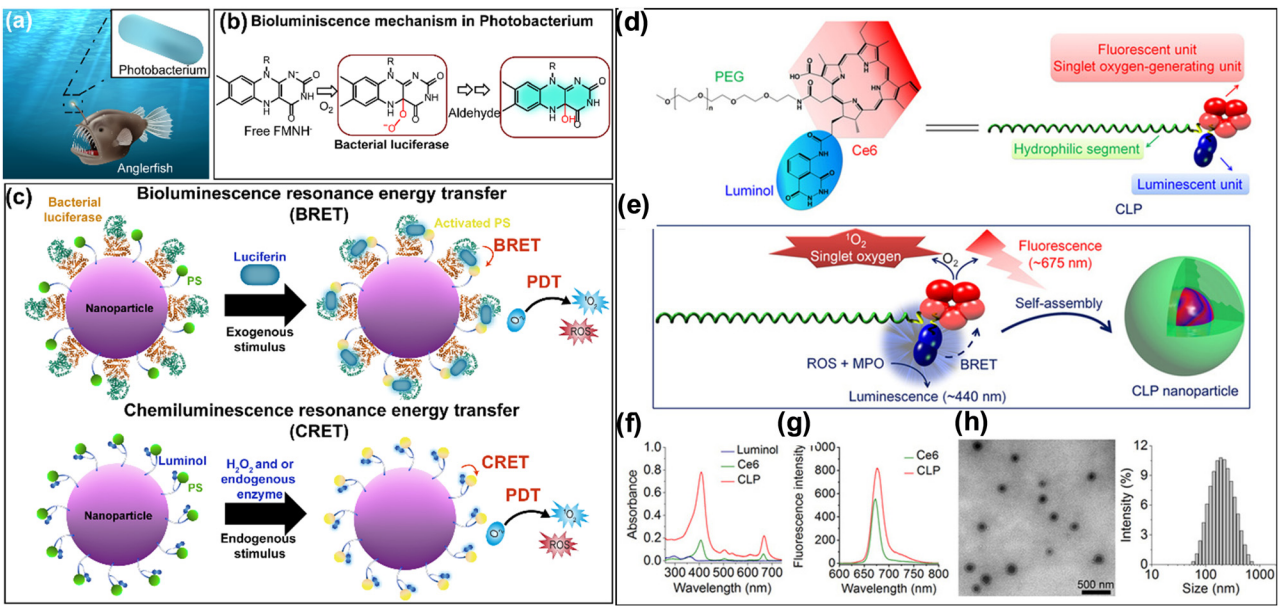

Fig. 9 (a) Drawing of an anglerfish with the glowing photobacterium inside the dangling lure. (b) The mechanism of bioluminescence driven by bacterial luciferase. The crystal structure of the bacterial luciferase was adapted from PDB entry 1LUC. (c) Schematic illustration of the designed photoactivatable nanoparticles with either a BRET or CRET self-illuminating process for PDT application. (d) Chemical structure and schematic illustration of the Ce6–Luminol–PEG (CLP) conjugate designed by Xu *et al.*[95] for inflammation imaging and self-illuminating PDT application. (e) Scheme of the self-assembly of the CLP conjugates. (f) The absorbance and fluorescence spectra of CLP assemblies compared to free Ce6. (h) TEM and DLS measurements of the CLP assemblies.[95] (d)–(h) were reprinted and adapted from ref. 95, Copyright 2019, American Association for the Advancement of Science.

 This journal is © The Royal Society of Chemistry 2025

Open Access Article. Published on 08 July 2025. Downloaded on 1/21/2026 5:41:23 PM.
This article is licensed under a Creative Commons Attribution-NonCommercial 3.0 Unported Licence.

As an example of self-illuminating PDT nanoplatforms based on the BRET process, Yang *et al.*[96] developed biodegradable PLGA poly(lactic-*co*-glycolic acid) (PLGA) nanoparticles doped with Rose Bengal as a photosensitizer and decorated with luciferase enzyme. These nanoparticles exhibited a hydrodynamic diameter of ~28 nm. Upon the administration of the luciferin substrate, the endogenously generated bioluminescence enabled the activation of the photosensitizer to generate ROS. On top of that, *in vivo* studies in a mouse model of hepatocellular carcinoma (H22) demonstrated the efficacy of the developed nanoplatform by significantly inhibiting the tumor growth by BRET–PDT, a process that occurs in the absence of external light.[96] Other studies on BRET–PDT have been described so far which consist of conjugating quantum dots[97] or polymer-based nanoparticles[96,98,99] with luminescent proteins including luciferase and horseradish peroxidase.[93] To overcome the problems of the *in vivo* toxicity encountered with conjugated quantum dot-based nanoparticles especially for long term therapy but also the separate administration of the enzymes and analytes, Xu *et al.*[95] developed biodegradable polymeric core–shell nanoparticles based on the self-assembly of Ce6–luminol–PEG_{2000} (CLP) conjugates. These nanoparticles are capable of chemiluminescent resonance energy transfer (CRET) upon their reaction with reactive oxygen species (ROS) and myeloperoxidase, which are produced in inflammatory sites or in the tumor microenvironment. This property facilitates the detection of inflammation and PDT against cancer. While chlorin e6 (Ce6) was used as a photosensitizer, luminol was conjugated to PEG polymer to function as a chemiluminescent compound.[100] The obtained core–shell nanoparticles exhibited a spherical shape with a mean hydrodynamic diameter of ~ 170 nm displaying reduced absorbance and fluorescence of the Ce6 photosensitizer due to their aggregation inside the core.[95] In addition, these nanoplatforms revealed their capability in generating luminescence *in vitro* under oxidative conditions with the appearance of two emission peaks at 450 nm and 675 nm corresponding to the fluorescence of luminol and Ce6 respectively. The authors demonstrated the efficiency of the developed nanoplatforms in fluorescence imaging in mice with a peritonitis model but also in PDT in mice bearing A549 xenografts.[95] Other studies based on CRET or BRET for PDT application were recently published in the cited reviews.[93,94,101] Besides the bioluminescence, some marine species such as sea snails known as abalones can cling tightly underwater to rock surfaces due their large muscular foot and their suction cup-like structure (Fig. 10a). Inspired by the latter, Song *et al.*[102] designed an adhesive photoactivatable drug delivery system for the treatment of periodontitis. To do so, the authors[102] developed photoactivatable microparticles exhibiting a cup-like structure and loaded with black phosphorus (BP) as a photothermal agent and minocycline hydrochloride (MH) antibiotic. The microparticles were synthesized through the photocuring of polyethylene glycol diacrylate (PEGDA) polymer with subsequent ionic cross-linking of sodium alginate (ALG) into calcium chloride solution using a microfluidic electrospray technology (Fig. 10b). The synthesized

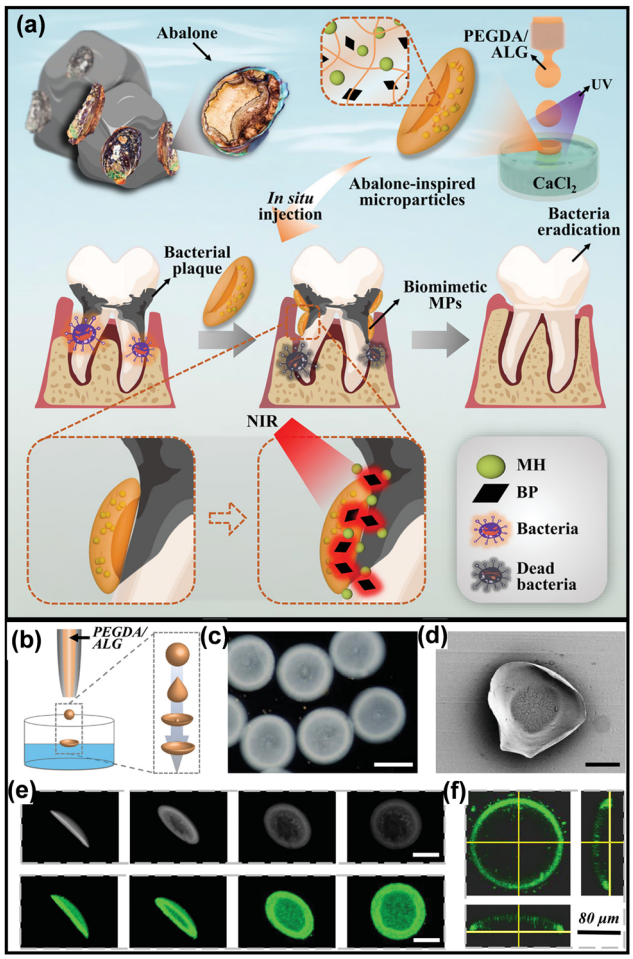

Fig. 10 (a) Scheme summarizing the design, preparation process and application of the abalone-inspired microparticles (MPs). (b) Schematic diagram of the preparation process of the microparticles. (c) Bright-field microscopic image of the MPs. Scale bars = 200 μm. (d) Scanning electron microscope (SEM) image of an isolated MP. Scale bars = 100 μm. (e) Digital and fluorescent images of a MP with different angles. Scale bars = 100 μm. (f) 3D confocal images of the FITC-loaded MPs outlining MPs' suction-cup structure. Adapted with permission from ref. 102, Copyright 2022, Wiley-VCH.

microparticles exhibited enhanced adhesive properties underwater on the teeth surface compared to conventional spherical microparticles. In addition, upon their illumination at 660 nm, the microparticles released minocycline antibiotic in a controlled manner and exhibited exceptional antibacterial activity *in vitro* and *in vivo* against *Porphyromonas gingivalis*, the agent of periodontitis.[102]

3.3. Bio-inspiration from anaerobic bacteria to improve PDT in hypoxic tumors

As explained above, PDT requires the presence of oxygen to produce reactive oxygen species that destruct cancer cells. However, solid tumors frequently exhibit conditions of hypoxia, defined as oxygen levels below 1% O_2 (10 000 PPM O_2; 10 μM O_2), a consequence of anaerobic metabolism.[103] Besides cancer, in bacterial infection and specially those related to biofilm, the

Open Access Article. Published on 08 July 2025. Downloaded on 1/21/2026 5:41:23 PM. This article is licensed under a Creative Commons Attribution-NonCommercial 3.0 Unported Licence.

oxygen is unevenly distributed within the biofilm, with very little amount of it at the bottom.[104] This phenomenon has the potential to compromise the efficacy of PDT. Various strategies have been proposed in order to overcome this kind of issue.[105] One of them is based on the bioinspiration from anaerobic bacteria.[106] Indeed, it has been demonstrated that anaerobic and facultative anaerobic bacteria, such as species of the genus *Clostridium* and *Salmonella*, can selectively invade tumor hypoxic regions and deliver anticancer drugs to destroy cancer cells.[107,108] In addition, when submitted to a hypoxic environment, such bacteria can scavenge superoxide radicals by the activity of superoxide reductase enzymes. Inspired by the tumor invasion mechanism by anaerobic bacteria as well as by their metabolism under hypoxic conditions, Qian *et al.*[106] have designed polymeric anaerobe-inspired nanovesicles (AI-NV) that are sensitive to hypoxic tumors and can generate ROS upon illumination through photodynamic reaction.[106] These AI-NVs are polymersomes (Fig. 11) which consist of three primary elements: (i) a light responsive diblock copolymer ((Ce6)-modified diblock copolymer PEG–poly(Ser-Ce6)), (ii) a ROS and hypoxia dual-responsive diblock copolymer (2-nitroimidazole (NI) with a thioether-modified diblock copolymer PEG–poly(Ser-S-NI)) and (iii) a hypoxia-sensitive prodrug (tirapazamine (TPZ)) loaded in the aqueous core.[106] After the intravenous administration of the bioinspired polymersomes (hydrodynamic diameter of 118 nm), they were expected to accumulate in the tumors through the enhanced permeability and retention (EPR) effect.[109] Afterwards, upon their illumination (λ = 650 nm), Ce6 photosensitizers generate singlet oxygen that can induce cancer cell death, and at the same time oxidize the thioether functional group of the PEG–poly(Ser-S-NI) polymer to PEG–poly(-Ser-SO_2-NI).[106] The hypoxic tumor environment as well as the continuous consumption of oxygen during this photodynamic process result in the formation of more hydrophilic PEG–poly(Ser-SO_2-AI) catalyzed by a series of nitroreductases through bioreduction in the hypoxic tumor. Such polymer modification will lead to vesicle dissociation with the subsequent release of tirapazamine (TPZ). The hypoxia-activatable prodrug TPZ, can then be activated to generate toxic hydroxyl and benzotriazinyl to oxidize radicals under low-oxygen conditions. *In vitro* and *in vivo* experiments on hepatocellular carcinoma (Heps) tumor-bearing mice indicated the efficiency of the anaerobe-inspired vesicles to induce apoptotic cell death and significantly inhibit tumor growth.

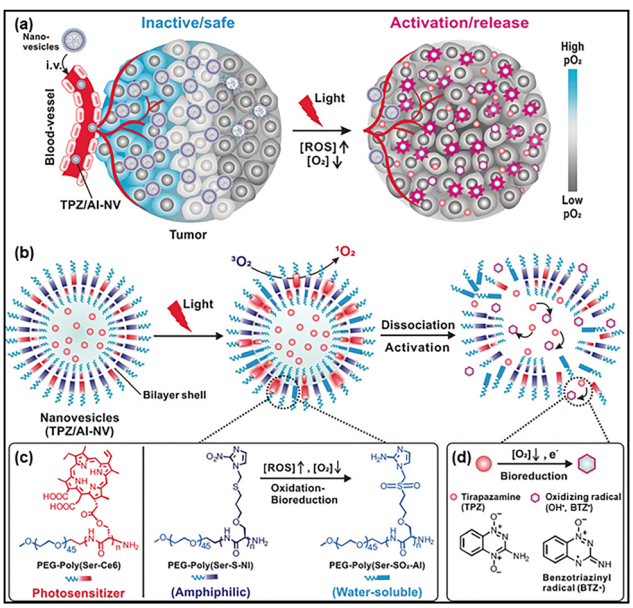

Fig. 11 (a) Scheme representing the anaerobe inspired nanovesicles TPZ/AI-NV. (b) Mechanism of activation of TPZ/AI-NV nanovesicles and simultaneous activation and dissociation through bioreduction of the prodrug. (c) The chemical structure of photosensitizer Ce6 modified diblock copolymer PEG–poly(Ser-Ce6); the ROS and hypoxia dual-sensitive diblock copolymer PEG–poly(Ser-S-NI). (d) The proposed mechanism of TPZ generating toxic oxidizing radical species under low-oxygen conditions. Adapted with permission from ref. 106, Copyright 2017, Wiley-VCH.

3.4. Bio-inspiration from melanin chromophores for the design of photoactivatable nanoparticles for biomedical applications

Melanin pigments are natural biopolymers of dark color that can be found in various parts of living organisms, such as the skin, eyes, hair, and brain. These pigments can also be found in other living organisms, including bacteria, fungi, plants, and squid. In humans, melanin pigments are produced by epidermal melanocytes, and their primary functions include imparting color to the skin and protecting it against UV light. Melanin pigments exhibit intriguing optical properties due to their broad absorption spectrum, which encompasses the UV-visible-NIR regions. These pigments contribute to various physiological functions, including radical scavenging, antioxidant properties, and metal ion chelation. Consequently, melanin has been proposed as an endogenous chromophore for photoacoustic imaging. However, the extraction of melanin pigments from natural sources is a complex process that necessitates several purification steps. Thus, synthetic methods for melanin-like polymers have been proposed, leading to the synthesis of polydopamine (PDA) polymer, which was first described by Swan *et al.*[110,111] in 1963 as an analog of natural melanins. However, significant attention has been drawn to PDA polymer since the discovery by Messersmith's group[112] of its coating and adhesion properties on a wide range of surfaces. These properties mimic the strong adhesive properties of marine mussel foot proteins on diverse wet surfaces. PDA coating layers or nanoparticles can be easily prepared by auto-oxidation of dopamine monomer under mild alkaline conditions.[113] Due to their melanin-like characteristics, PDA nanoparticles have emerged as versatile nanomaterials, exhibiting several intriguing properties, including biodegradability, biocompatibility, radical scavenging effect, high photothermal effect, and photoacoustic properties.[114] Numerous reviews have addressed the use of PDA nanoparticles and the diverse therapeutic approaches and combinations.[114–117] For instance, our group has developed a PDA-based nanoplatform for PTT and PDT bimodal therapy of esophageal cancer. These nanoplatforms entail the functionalization of the PDA nanoparticles with the PEG polymers bearing at their extremity

 This journal is © The Royal Society of Chemistry 2025

Open Access Article. Published on 08 July 2025. Downloaded on 1/21/2026 5:41:23 PM. This article is licensed under a Creative Commons Attribution-NonCommercial 3.0 Unported Licence.

trisulfonated-tetraphenyl porphyrin (TPPS3) photosensitizers, which are conjugated with thioketal as ROS-responsive linkers. The illumination of the obtained nanoparticles at 808 nm generated heat, while excitation at 590–642 nm led to the generation of ROS, following the release of the photosensitizer, thereby enhancing the photodynamic effect. This enabled successful PTT/PDT bimodal therapy *in vitro* against human squamous esophageal cells.[13]

4. Biohybridization of photoactivatable nanoconstructs with biological materials to improve their *in vivo* functionalities

4.1. Cell membrane biomimetic ghosts for improved safety and targeting ability of light-responsive nanomaterials

Even though phototherapy possesses many advantages, most of the photoactivatable nanomaterials suffer from short circulation time, targeting and specificity deficits. Normally, it is difficult to exert treatment solely on disease areas. Scientists worked on nanomaterial design to enhance targeting and pharmacokinetic properties for better delivery of phototherapeutic agents. However, a vast variety of materials cannot escape the human's immune system, leading to immune responses such as renal and liver clearance, resulting into inefficient treatment. Biomimetic camouflaging has emerged as a nanomaterial modification method that consists of the coating of the photoactive materials with cell membrane. For instance, membrane extracted from platelet cells, red blood cells, leucocytes, macrophages or cancer cells were recorded as camouflaging components (Fig. 12a) to engulf drug delivery systems to boost the accumulation, targeting, and release of an active molecule.[118] For example, platelets and red blood cell (RBC) membranes possess an integrin-associated protein CD47 marker, which decreases the susceptibility of RBCs to destruction by phagocytosis. Thus coating photoactive nanomaterials with these membranes enables the prolongation of their circulation time in the blood.[118] Coating photoactive nanomaterials with a leukocyte membrane enables recognition of the cancer cells. Whereas, the cancer cell membranes express some surface markers and adhesion molecules on their membrane thus enabling tumor targeting thanks to the homotypic binding to cancer cells.[119] Indeed, homotypic targeting, which is frequently observed in immune responses, tissue formation, and cell adhesion, is the innate capacity of cells to interact preferentially with cells of the same or similar types.[119,120] Although interesting, the membrane-based camouflage strategy encounters several hurdles, limiting their utilization in clinics due to the complexity of the membrane extraction process, purification and composition variability from batch to batch. For a more thorough description of the biomimetic camouflage of light-responsive nanomaterials, readers can refer to a recent review by Prasad *et al.*[118] In addition to the camouflaging properties offered by cell membrane ghosts, these latter can exhibit some functionalities thus enabling the multifunctional properties of the designed light-responsive nanoconstructs. Molecular chaperones are a class of proteins that assist and regulate protein conformational change within cells.[121] In particular, molecular chaperones can capture aberrant amyloid peptides while preventing their aggregation into toxic β-sheet fibrils. Moreover, they can depolymerize the amyloid fibrils into monomers.[122] Inspired by the molecular chaperones functionalities, Wang *et al.*[123] have designed erythrocyte membrane (EM) coated core–shell upconversion nanoparticles (UCNPs) loaded with curcumin as a photosensitizer (UCNP/Cur@EM) (Fig. 12b). The UCNPs were made as NaYF4,Yb,Tm@NaYF4, and were further modified with a silica layer and a mesoporous silica layer to load the curcumin photosensitizer. The obtained UCNPs were further coated with EMs by extrusion, which yielded UCNP/Cur@EM with an average hydrodynamic diameter of ~460 nm. The interest in EM coating was not to obtain camouflage properties but rather to act as nanobait to attract Aβ peptides, which restrains in turn the Aβ aggregation. Besides, upon their illumination at 980 nm the generated ROS will degrade the preformed Aβ fibrils and aggregates. The developed bioinspired light-responsive nanoparticles have proven their efficiency *in vivo* by decreasing the Aβ deposits while improving the memory deficits and the cognitive functions in the APP/PS1 transgenic mouse model.[123] In addition to the coating of photoactivatable nanomaterials with biomimetic membranes, other targeting strategies have been adopted. These include the use of full-length antibodies, engineered proteins, and natural ligands for photodynamic therapy (PDT)[124] or photothermal therapy (PTT)[125] applications. However, a single receptor targeting approach is not always sufficient due to receptor heterogeneity in cancer, which may lead to treatment resistance. To address this challenge, Bano *et al.*[126] designed a novel photoimmuno-nanoconjugate (TR-PIN) nanoplatform which can target three receptors simultaneously for PDT applications. This nanoplatform is based on liposomal nanoconstructs that incorporate benzoporphyrin derivative-lipid conjugates. The liposomes were then functionalized at the PEG extremity with cetuximab, holo-transferrin, and trastuzumab. These macromolecules can target specifically epidermal growth factor receptor (EGFR), transferrin receptor (TfR), and human epidermal growth factor receptor 2 (HER-2), respectively.[126] The authors demonstrated the efficacy of this approach by enhancing the binding of these liposomes to cancer cells and improving their photodestruction in *in vitro* models compared to monofunctionalized nanoplatforms.[126]

4.2. Cyanobacteria biohybridization to improve PDT in hypoxic tumors

Cyanobacteria are a class of photosynthetic bacteria also known as "blue-green algae"[128] which can produce oxygen by photosynthesis like green plants. Interestingly, some species of cyanobacteria are biocompatible which makes them ideal candidates for the design of light-activatable microplatforms with light-induced oxygen-producing abilities in hypoxic tumors or infections. Indeed, Qi *et al.*[129] attached black

Open Access Article. Published on 08 July 2025. Downloaded on 1/21/2026 5:41:23 PM.
This article is licensed under a Creative Commons Attribution-NonCommercial 3.0 Unported Licence.

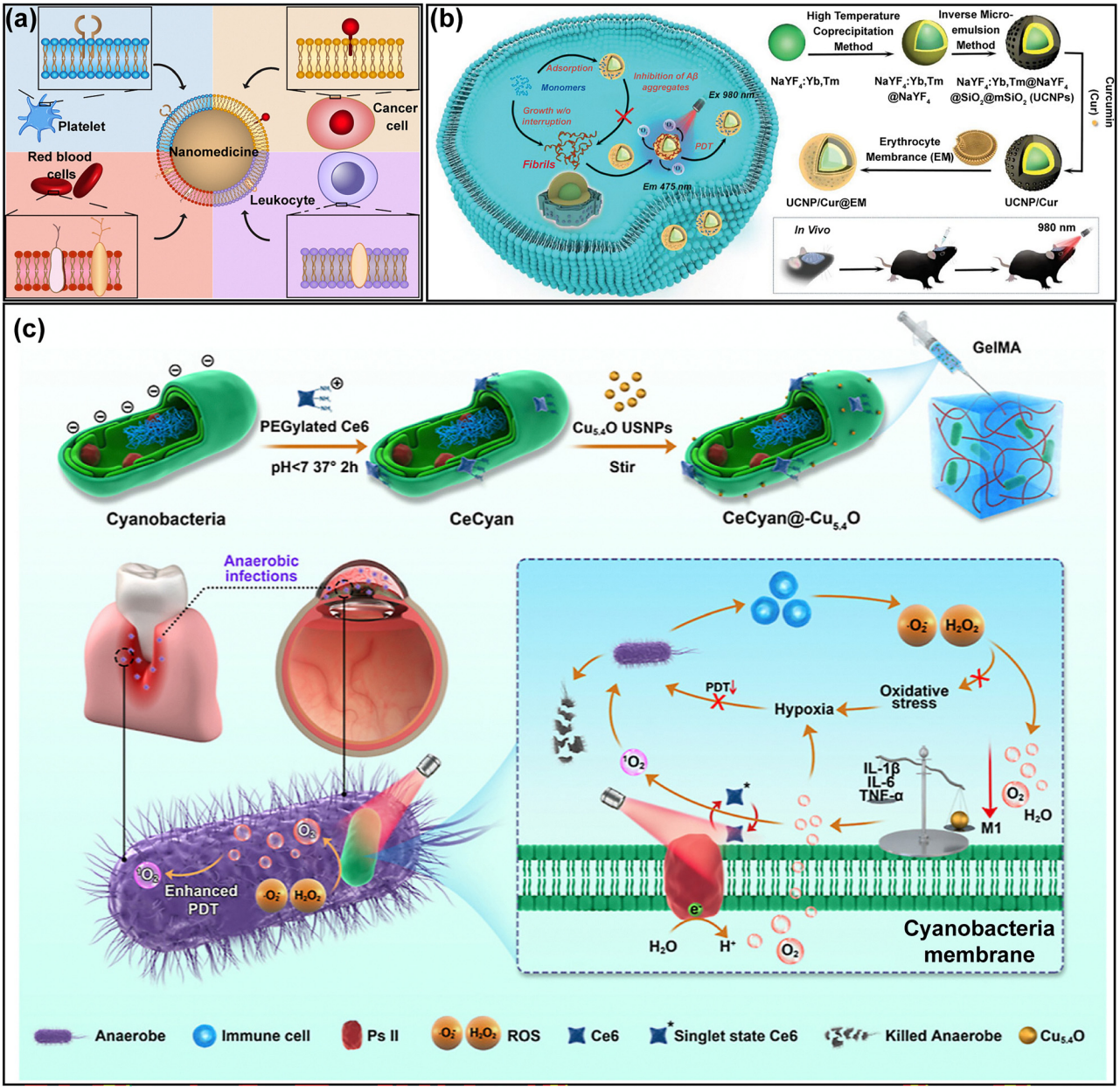

Fig. 12 (a) Scheme representing the main strategies that have been used in the 'camouflage' of light-responsive nanoparticles. (b) Schematic illustration of the preparation method of the biomimetic upconversion nanobait-based PDT for the inhibition of Aβ aggregates. Adapted with permission from ref. 123, Copyright 2024 Wiley-VCH. (c) Schematic representation of the fabrication of CeCyan–$Cu_{5.4}O$ and its application in the treatment of anaerobic bacterial infections. Adapted with permission from ref. 127, Copyright Elsevier 2022.

phosphorus nanosheets (BPNSs) as photosensitizers to the membrane of a cyanobacteria strain (*Synecoccus elongatus*, PCC7942)). Upon illumination of the system at 660 nm the hybridized cyanobacteria generate oxygen through photosynthesis, while the BPNSs transform the generated oxygen into cytotoxic singlet oxygen species. The authors demonstrated the efficiency of the developed system *in vivo* on 4T1 tumor xenograft models following intratumor injection. Similarly, Wang *et al.*[127] hybridized cyanobacteria with Ce6 photosensitizer and ultrasmall $Cu_{5.4}O$ nanoparticles (USNPs) to design a self-oxygenated photodynamic platform (CeCycn–$Cu_{5.4}O$) for the treatment of anaerobic infections and the tissue reparation. While Ce6 molecules play the role of photosensitizer, the USNPs serve as nano-enzymes with high efficiency catalase activity to reduce the oxidative stress damage accompanying the bacterial infection. The authors demonstrated the efficiency of the hybridized cyanobacteria platform *in vivo* in both anaerobic infectious keratitis and periodontitis animal models.[127]

4.3. Biohybridization with hemoglobin or myoglobin for the improvement of PDT or radiotherapy in hypoxic tumors

Hemoglobin (Hb) is the protein present in red blood cells, which can bind four oxygen molecules in a reversible manner to ensure adequate tissue oxygenation and oxygen transport.

 This journal is © The Royal Society of Chemistry 2025

Open Access Article. Published on 08 July 2025. Downloaded on 1/21/2026 5:41:23 PM. This article is licensed under a Creative Commons Attribution-NonCommercial 3.0 Unported Licence.

This important functionality has inspired researchers to use hemoglobin as an oxygen carrier to improve the photodynamic therapy outcomes for hypoxic tumors.[105] However free hemoglobin suffers from poor stability under physiological conditions and a short circulation time. Therefore, authors have suggested loading or conjugating Hb into drug delivery systems in combination with photosensitizers to increase the production of singlet oxygen and thus the PDT efficiency against hypoxic tumors.[130] In addition, due to the rapid growth rate of cancer cells, they can upregulate proteins related to iron uptake. Therefore, decorating drug delivery systems such as liposomes with hemoglobin facilitates their specific internalization into cancer cells. Consequently, such nanoplatform allows improved PDT efficiency with specific targeting ability towards cancer cells.[131] Besides hemoglobin, myoglobin (Mb), a cytoplasmic hemoprotein, is found in both cardiac and skeletal muscles. This hemoprotein consists of a single polypeptide chain. It has the capacity to bind reversibly oxygen *via* its heme residue (Fig. 13a). This binding process enables the storage of oxygen in muscles. As with hemoglobin, myoglobin

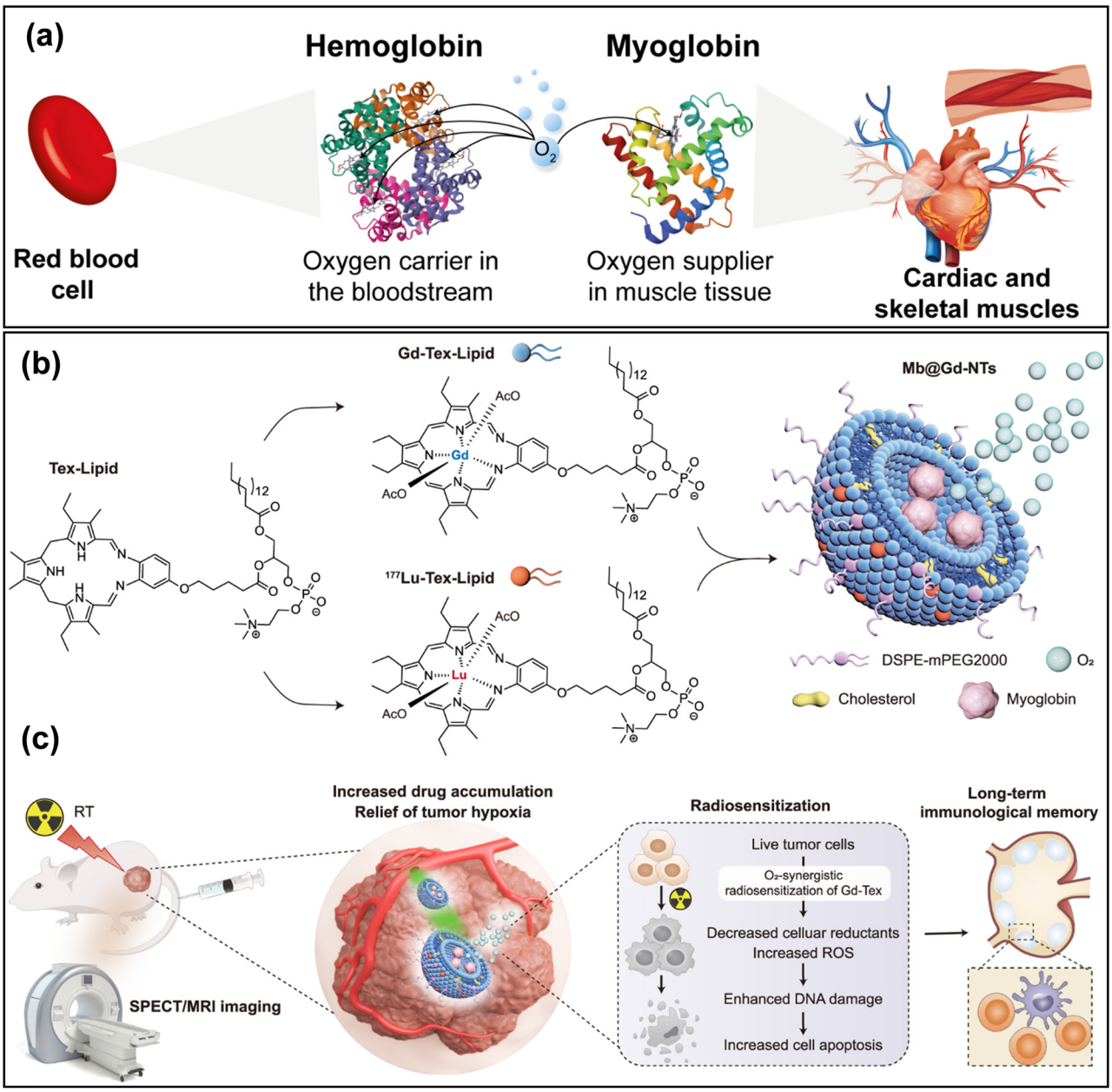

Fig. 13 (a) Schematic representation of the sources and the role of hemoglobin (PDB entry 2DHB) and myoglobin (PDB entry 1mbn). (b) Chemical structures of the Tex–lipid conjugates coordinated either with gadolinium ion (Gd^{3+}) or lutenium ($^{177}Lu^{3+}$) and their formulation with myoglobin. (c) Scheme representing the expected effect following the intravenous injection of the Mb@177Lu/Gd-NTs formulations with the possibility of SPECT/MRI dual modality imaging to monitor the drug delivery in real time. The myoglobin enhances the radiosensitization effect thanks to the release of oxygen. Adapted with permission from ref. 136, Copyright 2023 Springer Nature.

Open Access Article. Published on 08 July 2025. Downloaded on 1/21/2026 5:41:23 PM. This article is licensed under a Creative Commons Attribution-NonCommercial 3.0 Unported Licence.

has been utilized as an effective nanocarrier for porphyrin derivatives in photodynamic therapy (PDT) applications.[132,133] For instance, Komatsu's group[134] has recently developed a heme-free fused protein comprising Mb and human serum albumin (HSA). This protein was termed ''apoMb-HSA.'' The latter was further loaded with zinc(II)-phthalocyanine (ZnPc) photosensitizer, resulting in ZnPc-substituted Mb-HSA (ZnPcMb–HSA). The obtained complex exhibited a higher propensity for generating singlet oxygen in comparison to ZnPc–HSA, yet it demonstrated comparable capabilities to those of ZnPcMb. Notably, the fused Mb–HSA protein reduced the dissociation of the ZnPC from the heme pocket in comparison to ZnPCMb in simulated plasma conditions. The cellular uptake and the PDT efficiency were further evaluated *in vitro* in four cell lines: HeLa (human cervical cancer), MCF-7 (human breast cancer), A549 (human lung cancer), and NCI-N87 (human gastric cancer). The obtained results indicated the dissociation of the ZnPC from the protein components and its efficient internalization inside the cells. Following illumination, ZnPcMb–HSA demonstrated efficient photosensitizing properties, exhibiting IC50 values ranging from 0.1 to 0.5 μM, depending on the cell type. Radiodynamic therapy (RDT) is another therapeutic modality that employs a comparable approach to PDT. RDT is based on the utilization of high-energy radiation in conjunction with porphyrin derivatives also known as radiosensitizers. One of the mechanisms of RDT, is the ionization of the photosensitizers, thereby rendering them capable of reacting with surrounding molecules particularly oxygen and H_2O to generate cytotoxic $O_2^{\bullet -}$ or $^{\bullet}OH$ radicals.[135] Hence, as in the case of PDT, the RDT efficiency depends on the oxygenation level of the tissues. Inspired by the myoglobin role and with the objective of enhancing the RDT efficiency of the Gadolinium ion (Gd^{3+})-coordinated texaphyrin (Gd-Tex) radiosensitizer, Ma *et al.*[136] developed a novel organic nanoplatform loaded with myoglobin as an oxygen carrier (Fig. 13b). To do so, the authors synthesized a novel lipid-gadolinium-coordinated texaphyrin building block (Gd–Tex–lipid). In a manner analogous to lipid–porphyrin conjugates, Gd–Tex–lipids can self-assemble into liposomal-like structures, manifesting a high density of texaphyrin molecules within the bilayer (Fig. 13b). The utilization of novel building blocks at a mass percentage of approximately 49% in combination with DSPC, cholesterol, and $DSPE–PEG_{2000}$ enabled the authors to engineer a novel liposomal nanoplatform (hydrodynamic diameter ~120 nm) that encapsulates myoglobin within its core (Mb@Gd-NTs). The developed nanoplatforms demonstrated the capacity to release oxygen *in vitro* in a manner characterized by steady release profile kinetics. In addition, the liposomes were doped with lutenium ($^{177}Lu^{3+}$) chelated texaphyrin building blocks (Lu–Tex–lipid) to enable additional single photon emission computed tomography (SPECT) imaging Fig. 13b). Following X-ray irradiation at a dose of 2 Gy, the MbO2@Gd-NTs demonstrated the capacity to produce ROS in Lewis lung cancer (LLC) cells with high efficiency. This process resulted in a significant reduction in cell survival percentage, reaching 99.3% compared to other controls, including Gd-NTs devoid of MbO_2. The developed nanoplatform exhibited a significant *in vivo* radiosensitization effect and a synergistic effect in the LLC-bearing mice model when compared to Gd-NTs or Mb@NTs (Fig. 13c). This work unequivocally demonstrated the impact of oxygen on enhancing radiosensitization efficacy.[136]

5. DNA scaffolds to improve the light interaction with chromophores and their delivery

Deoxyribonucleic acid (DNA) is a well-known biomolecule, which encodes genetic information. It exhibits a double helix structure composed of two polynucleotide chains that interact with complementary principle *via* hydrogen bonds between bases pairs: with adenine always pairing with thymine, and guanine always pairing with cytosine. This structure has inspired intensive research for the design of DNA-templated photonic materials mainly for artificial light harvesting systems[137] or the development of biosensors,[138] where the position, the orientation or the dynamics of the chromophores can be finely tuned and predicted by the DNA structure. Besides light-harvesting applications, DNA nanotechnology has also been applied to the design of light–responsive nanomedicines.[16,139] Indeed, photothermal and photodynamic therapies are the main biomedical applications that have been advanced by DNA nanotechnology. Using DNA scaffolds in phototherapy has been mainly adopted either to (i) organize the chromophores and photothermal agents, thus their interaction with light or (ii) to improve internalization inside the cancer cells and also for tumor targeting. Zhuang *et al.*[140] have used triangular-shaped DNA origami structures as an efficient delivery nanosystem of a hydrophobic photosensitizer 3,6-bis[2-(1-methylpyridinium) ethynyl]-9-pentylcarbazole diiodide (BMEPC) for photodynamic therapy and fluorescence imaging. The DNA origami structures (outer triangular edge ~115 nm, height ~2 nm) were first self-assembled with M13 phage DNA, staple strands and then loaded with BMEPC chromophores. Thanks to their positive charge, they were easily intercalated into the DNA base pairs. Such loading restricted the intramolecular rotation of BMPEC molecules while increasing their fluorescence quantum yield and their photodynamic efficiency. This nanoplatform has proven its higher efficiency in photodynamic therapy and one-photon fluorescence imaging *in vitro* against MCF-7 cancer cells compared to the carrier-free BMEPC (Fig. 14a). Similarly, Song *et al.*[141] have reported the design of multifunctional self-assembled MUC-1 triangular DOX-AuNR (MODA) DNA origami nanostructures to combat resistant breast cancer cells (MCF7/ADR) by a combined chemo/photothermal therapy. The DNA origami was loaded with doxorubicin through base pair intercalation and with gold nanorods (AuNRs) which were incorporated through DNA hybridization. In addition, this DNA origami was further functionalized with MUC-1 aptamer to target mucin proteins, which are overexpressed on the surface of tumor epithelial cells (Fig. 14b). Upon cell illumination at 808 nm (4.5 W cm^{-2}), the photothermal effect inhibited the ATP-dependent P-glycoprotein drug efflux pump on the cell membrane thus increasing the MCF7/ADR sensitivity to

 This journal is © The Royal Society of Chemistry 2025

Open Access Article. Published on 08 July 2025. Downloaded on 1/21/2026 5:41:23 PM.
This article is licensed under a Creative Commons Attribution-NonCommercial 3.0 Unported Licence.

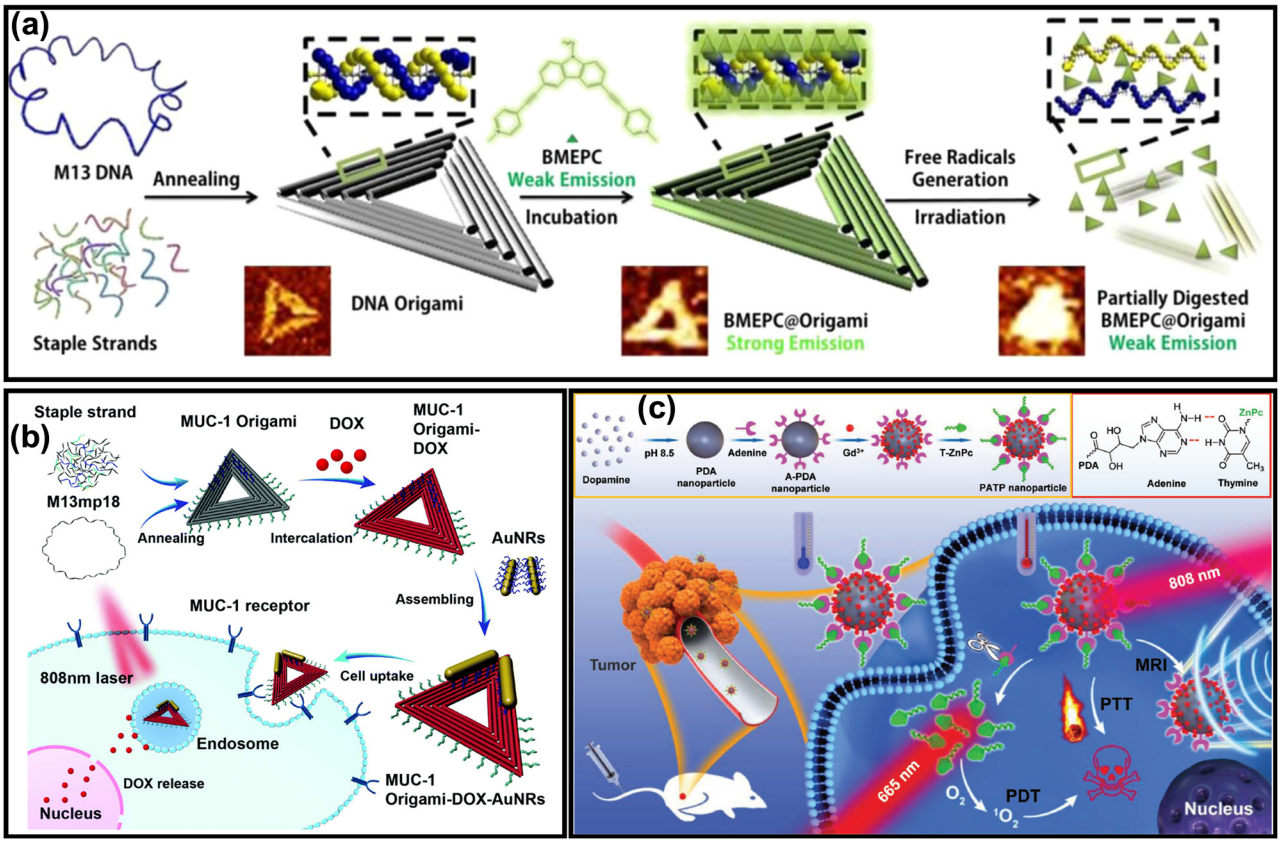

Fig. 14 (a) The preparation method of DNA origami exhibiting triangular shape and loaded with BMEPC. (b) Schematic representation of the preparation route of triangular-shaped DNA origami loaded with gold nanorods and doxorubicin for synergistic PTT and chemotherapy. (c) Schematic illustration of the polydopamine nanoparticles conjugated with phthalocyanine photosensitizer *via* a pairing strategy and photosensitizer releasing process induced by the photothermal effect. Adapted with permission from ref. 147, Copyright 2018 Wiley-VCH.

doxorubicin. Other studies have been conducted for triangular DNA origami development where gold nanorods were attached at specific designated locations thus enabling improved two-photon cell imaging *in vitro*,[142] photoacoustic imaging[143] and *in vivo* photothermal therapy.[142,143] In addition to the DNA origami nanostructures, molecular beacons (MBs) are simpler DNA hairpin structures that are specifically used for the design of activatable fluorescent probes or photosensitizers.[16,20,144] These probes contain a fluorescent molecule or a photosensitizer at one end and a quencher molecule at the other. The close proximity between the photosensitizer and the quencher prohibits the fluorescence or the singlet oxygen generation until the linker between them is enzymatically cleaved at the site of treatment. Several protease-cleavable PDT beacons have been designed by using Pyropheophorbide-a (Pyro-a) as a photosensitizer which was conjugated *via* a metalloproteinase-responsive linker to black hole quencher 3 (BHQ3).[20,145,146] These Pyro-BHQ3 PDT beacons have proven their efficiency *in vivo* on multiple tumor mouse models overexpressing metalloproteinase MMP-7.[146] Besides the use of DNA nanostructures as the delivery system for photosensitizers or photothermal agents, the thermal behavior of DNA has inspired researchers to release the photosensitizer upon reaching a threshold temperature. For example, Zhan *et al.*[147] designed photothermal polydopamine (PDA) nanoparticles functionalized with adenine molecules (Fig. 14c). These nanoparticles enabled the specific adsorption of thymine-modified zinc–phthalocyanine photosensitizers on their surface thus yielding bimodal photothermal/photodynamic nanoplatforms. Moreover, similar to DNA whose bases will dissociate upon heating, the illumination of the PDA nanoparticles generated heat upon their illumination at 808 nm thanks to their photothermal properties. The generated heat led to the dissociation and release of the zinc–phthalocyanine molecules in the tumor cells enhancing thus their photodynamic outcome upon illumination at 665 nm.[147]

6. Conclusions and perspectives

In this review, we attempted to highlight recent advances in the development of nature-inspired photoactivatable nanoconstructs for biomedical applications. Natural systems can provide inspiration for designing or improving the functionalities of photoactivatable nanomedicines in several applications including drug delivery, bioimaging and photodynamic therapy. The unique ability of natural light-harvesting systems to collect photons under dim conditions, but also to provide photoprotection under intense sunlight, led scientists to explore these features for the design of photoactivatable

Open Access Article. Published on 08 July 2025. Downloaded on 1/21/2026 5:41:23 PM. This article is licensed under a Creative Commons Attribution-NonCommercial 3.0 Unported Licence.

nanoconstructs with enhanced light absorption in the NIR region and for the design of activatable photodynamic therapy respectively. In addition to these systems, thylakoids, jellyfish, anglerfish, anaerobic bacteria, melanin pigments, cell membranes, cyanobacteria, hemoglobin, and DNA scaffolds can provide significant improvements in the functionalities of light-responsive nanomedicines for either diagnosis or treatment. However, there are still unexplored systems and phenomenon in nature that need to be understood to offer immense potential for more accurate and efficient light-based therapies. Despite their potential, challenges such as biocompatibility, scaling and *in vivo* stability require further improvements to ensure clinical translation. However, the advent of nanotechnology, biomaterials and photomedicine might make the development of scalable, bioinspired photoactivatable nanomedicines a conceivable prospect. In conclusion, it should be emphasized that the design of photoactivatable bioinspired nanomedicines should be kept as simple as possible for the purposes of scaling and clinical applications.

Conflicts of interest

There are no conflicts to declare.

Data availability

No primary research results, software or code have been included and no new data were generated or analysed as part of this review.

Acknowledgements

This work is partially supported by the ANR JCJC Grant (Project-ANR-19-CE09-0015), by the graduate school ''Health and Drug Sciences'' (HeaDS) in the frame of ''Junior Project leader'' call, by the CNRS through the MITI interdisciplinary programs (Défi Auto-organisation) and through CNRS 80 PRIME, 2020 CNRS – University of Toronto Joint Call. This work is part of the PHORTUNA project of PEPR LUMA and was supported by the French National Research Agency, as a part of the France 2030 program, under grant ANR-24-EXLU-0011.

Notes and references

1 P. M. Tiwari, S. S. Bawage and S. R. Singh, in *Applications of Nanoscience in Photomedicine*, ed. M. R. Hamblin and P. Avci, Chandos Publishing, Oxford, 2015, pp. 249–266, DOI: 10.1533/9781908818782.249.
2 R. Ackroyd, C. Kelty, N. Brown and M. Reed, *Photochem. Photobiol.*, 2001, **74**, 656–669.
3 M. F. Holick, J. A. MacLaughlin, J. A. Parrish and R. R. Anderson, in *The Science of Photomedicine*, ed. J. D. Regan and J. A. Parrish, Springer US, Boston, MA, 1982, pp. 195–218, DOI: 10.1007/978-1-4684-8312-3_7.
4 T. H. Maiman, *Nature*, 1960, **187**, 493–494.
5 N. S. Kapany, N. A. Peppers, H. C. Zweng and M. Flocks, *Nature*, 1963, **199**, 146–149.
6 L. Goldman, D. J. Blaney, D. J. Kindel, Jr. and E. K. Franke, *J. Invest. Dermatol.*, 1963, **40**, 121–122.
7 L. Goldman, D. J. Blaney, D. J. Kindel, Jr., D. Richfield and E. K. Franke, *Nature*, 1963, **197**, 912–914.
8 L. Goldman, D. J. Blaney, D. J. Kindel, Jr., M. F. Richfield, P. Owens and E. L. Homan, *J. Invest. Dermatol.*, 1964, **42**, 247–251.
9 J. M. A. Q. Peng, in *Photodynamic Therapy*, ed. T. Patrice, The Royal Society of Chemistry, Cambridge, 2003, ch. 1, pp. 1–18.
10 X. Li, J. F. Lovell, J. Yoon and X. Chen, *Nat. Rev. Clin. Oncol.*, 2020, **17**, 657–674.
11 J. Massiot, W. Abuillan, O. Konovalov and A. Makky, *Biochim. Biophys. Acta, Biomembr.*, 2022, **1864**, 183812.
12 J. Massiot, V. Rosilio and A. Makky, *J. Mater. Chem. B*, 2019, **7**, 1805–1823.
13 I. Zmerli, N. Ibrahim, P. Cressey, S. Denis and A. Makky, *Mol. Pharmaceutics*, 2021, **18**, 3623–3637.
14 S. He, J. Song, J. Qu and Z. Cheng, *Chem. Soc. Rev.*, 2018, **47**, 4258–4278.
15 G. Hong, A. L. Antaris and H. Dai, *Nat. Biomed. Eng.*, 2017, **1**, 0010.
16 X. Zhou, S. Lin and H. Yan, *J. Nanobiotechnol.*, 2022, **20**, 257.
17 V. Balevičius, K. F. Fox, W. P. Bricker, S. Jurinovich, I. G. Prandi, B. Mennucci and C. D. P. Duffy, *Sci. Rep.*, 2017, **7**, 13956.
18 M. H. Himel, B. Sikder, T. Ahmed and S. M. Choudhury, *Nanoscale Adv.*, 2023, **5**, 596–614.
19 J. Liu, S. S. Liew, J. Wang and K. Pu, *Adv. Mater.*, 2022, **34**, 2103790.
20 K. M. Harmatys, M. Overchuk and G. Zheng, *Acc. Chem. Res.*, 2019, **52**, 1265–1274.
21 S. Matsubara and H. Tamiaki, *J. Photochem. Photobiol., C*, 2020, **45**, 100385.
22 P. D. Frischmann, K. Mahata and F. Würthner, *Chem. Soc. Rev.*, 2013, **42**, 1847–1870.
23 Y. Kimura, K. Tani, M. T. Madigan and Z.-Y. Wang-Otomo, *J. Phys. Chem. B*, 2023, **127**, 6–17.
24 G. T. Oostergetel, H. van Amerongen and E. J. Boekema, *Photosynth. Res.*, 2010, **104**, 245–255.
25 M. Kasha, *Radiat. Res.*, 1963, **20**, 55–70.
26 N. J. Hestand and F. C. Spano, *Acc. Chem. Res.*, 2017, **50**, 341–350.
27 F. Würthner, T. E. Kaiser and C. R. Saha-Möller, *Angew. Chem., Int. Ed.*, 2011, **50**, 3376–3410.
28 E. E. Jelley, *Nature*, 1936, **138**, 1009–1010.
29 E. E. Jelley, *Nature*, 1937, **139**, 631.
30 G. Scheibe, L. Kandler and H. Ecker, *Naturwissenschaften*, 1937, **25**, 75.
31 F. Witte, P. Rietsch, S. Sinha, A. Krappe, J.-O. Joswig, J. P. Götze, N. Nirmalananthan-Budau, U. Resch-Genger, S. Eigler and B. Paulus, *J. Phys. Chem. B*, 2021, **125**, 4438–4446.

 This journal is © The Royal Society of Chemistry 2025

Open Access Article. Published on 08 July 2025. Downloaded on 1/21/2026 5:41:23 PM. This article is licensed under a Creative Commons Attribution-NonCommercial 3.0 Unported Licence.

32 J.-Q. Cai, X.-M. Liu, Z.-J. Gao, L.-L. Li and H. Wang, *Mater. Today*, 2021, **45**, 77–92.
33 T. Mirkovic, E. E. Ostroumov, J. M. Anna, R. Van Grondelle, Govindjee and G. D. Scholes, *Chem. Rev.*, 2017, **117**, 249–293.
34 N.-U. Frigaard, D. Voigt Ginny and A. Bryant Donald, *J. Bacteriol.*, 2002, **184**, 3368–3376.
35 S. K. Saikin, Y. Khin, J. Huh, M. Hannout, Y. Wang, F. Zare, A. Aspuru-Guzik and J. K.-H. Tang, *Sci. Rep.*, 2014, **4**, 5057.
36 M. Higuchi-Takeuchi and K. Numata, *Front. Bioeng. Biotechnol.*, 2019, **7**, 1–8.
37 R. J. Cogdell, T. D. Howard, N. W. Isaacs, K. McLuskey and A. T. Gardiner, *Photosynth. Res.*, 2002, **74**, 135–141.
38 G. D. Scholes and G. Rumbles, *Nat. Mater.*, 2006, **5**, 683–696.
39 G. D. Scholes, G. R. Fleming, A. Olaya-Castro and R. van Grondelle, *Nat. Chem.*, 2011, **3**, 763–774.
40 R. J. Cogdell, N. W. Isaacs, A. A. Freer, T. D. Howard, A. T. Gardiner, S. M. Prince and M. Z. Papiz, *FEBS Lett.*, 2003, **555**, 35–39.
41 K. K. Ng, M. Shakiba, E. Huynh, R. A. Weersink, Á. Roxin, B. C. Wilson and G. Zheng, *ACS Nano*, 2014, **8**, 8363–8373.
42 J. F. Lovell, C. S. Jin, E. Huynh, H. Jin, C. Kim, J. L. Rubinstein, W. C. Chan, W. Cao, L. V. Wang and G. Zheng, *Nat. Mater.*, 2011, **10**, 324–332.
43 J. Massiot, V. Rosilio, N. Ibrahim, A. Yamamoto, V. Nicolas, O. Konovalov, M. Tanaka and A. Makky, *Chem. - Eur. J.*, 2018, **24**, 19179–19194.
44 K. K. Ng, R. A. Weersink, L. Lim, B. C. Wilson and G. Zheng, *Angew. Chem., Int. Ed.*, 2016, **55**, 10003–10007.
45 L.-G. Bronstein, Á. Tóth, P. Cressey, V. Rosilio, F. Di Meo and A. Makky, *Nanoscale*, 2022, **14**, 7387–7407.
46 D. M. Charron, G. Yousefalizadeh, H. H. Buzzá, M. A. Rajora, J. Chen, K. G. Stamplecoskie and G. Zheng, *Langmuir*, 2020, **36**, 5385–5393.
47 L. Cui, D. Tokarz, R. Cisek, K. K. Ng, F. Wang, J. Chen, V. Barzda and G. Zheng, *Angew. Chem., Int. Ed.*, 2015, **54**, 13928–13932.
48 L.-G. Bronstein, P. Cressey, W. Abuillan, O. Konovalov, M. Jankowski, V. Rosilio and A. Makky, *J. Colloid Interface Sci.*, 2022, **611**, 441–450.
49 P. Cressey, L.-G. Bronstein, R. Benmahmoudi, V. Rosilio, C. Regeard and A. Makky, *Int. J. Pharm.*, 2022, **623**, 121915.
50 P. Cressey, W. Abuillan, N. Ibrahim, J. Alhoussein, O. Konovalov, G. Zheng and A. Makky, *Chem. Phys. Chem.*, 2023, **24**, e202200687.
51 J. M. Alhoussein, M. Khatia, T. Ho, A. Elkihel, P. Cressey, Á. Tóth, A. Qian, M. Hery, J. Vergnaud, S. Domenichini, F. Di Meo, J. Chen, G. Zheng and A. Makky, *J. Controlled Release*, 2025, **381**, 113621.
52 D. Wang, L. Niu, Z.-Y. Qiao, D.-B. Cheng, J. Wang, Y. Zhong, F. Bai, H. Wang and H. Fan, *ACS Nano*, 2018, **12**, 3796–3803.
53 J. Otsuki, *J. Mater. Chem. A*, 2018, **6**, 6710–6753.
54 Y. Tian, R. Camacho, D. Thomsson, M. Reus, A. R. Holzwarth and I. G. Scheblykin, *J. Am. Chem. Soc.*, 2011, **133**, 17192–17199.
55 Y. Saga and H. Tamiaki, *J. Biosci. Bioeng.*, 2006, **102**, 118–123.
56 A. Egawa, T. Fujiwara, T. Mizoguchi, Y. Kakitani, Y. Koyama and H. Akutsu, *Proc. Natl. Acad. Sci. U. S. A.*, 2007, **104**, 790–795.
57 K. K. Ng, M. Takada, K. Harmatys, J. Chen and G. Zheng, *ACS Nano*, 2016, **10**, 4092–4101.
58 K. M. Harmatys, J. Chen, D. M. Charron, C. M. MacLaughlin and G. Zheng, *Angew. Chem., Int. Ed.*, 2018, **57**, 8125–8129.
59 M. Su, S. Li, H. Zhang, J. Zhang, H. Chen and C. Li, *J. Am. Chem. Soc.*, 2019, **141**, 402–413.
60 J. Chmeliov, A. Gelzinis, E. Songaila, R. Augulis, C. D. P. Duffy, A. V. Ruban and L. Valkunas, *Nat. Plants*, 2016, **2**, 16045.
61 R. Croce and H. van Amerongen, *Nat. Chem. Biol.*, 2014, **10**, 492–501.
62 G. Obaid, W. Jin, S. Bano, D. Kessel and T. Hasan, *Photochem. Photobiol.*, 2019, **95**, 364–377.
63 Y. Li, R. C. H. Wong, X. Yan, D. K. P. Ng and P.-C. Lo, *ACS Appl. Bio Mater.*, 2020, **3**, 5463–5473.
64 M. A. Azagarsamy, D. L. Alge, S. J. Radhakrishnan, M. W. Tibbitt and K. S. Anseth, *Biomacromolecules*, 2012, **13**, 2219–2224.
65 X. Li, S. Lee and J. Yoon, *Chem. Soc. Rev.*, 2018, **47**, 1174–1188.
66 Y. Xu, R. Liu, R. Li, X. Zhi, P. Yang, L. Qian, D. Sun, L. Liu and Z. Dai, *ACS Nano*, 2023, **17**, 16192–16203.
67 H. Hashimoto, Y. Sugai, C. Uragami, A. T. Gardiner and R. J. Cogdell, *J. Photochem. Photobiol., C*, 2015, **25**, 46–70.
68 D. Accomasso, G. Londi, L. Cupellini and B. Mennucci, *Nat. Commun.*, 2024, **15**, 847.
69 L. Cupellini, D. Calvani, D. Jacquemin and B. Mennucci, *Nat. Commun.*, 2020, **11**, 662.
70 T. A. Moore, D. Gust and A. L. Moore, *Pure Appl. Chem.*, 1994, **66**, 1033–1040.
71 J. Chen, K. Stefflova, M. J. Niedre, B. C. Wilson, B. Chance, J. D. Glickson and G. Zheng, *J. Am. Chem. Soc.*, 2004, **126**, 11450–11451.
72 J. Gao, H. Wang, Q. Yuan and Y. Feng, *Front. Plant Sci.*, 2018, **9**, 357.
73 N. Sewelam, N. Jaspert, K. Van Der Kelen, V. B. Tognetti, J. Schmitz, H. Frerigmann, E. Stahl, J. Zeier, F. Van Breusegem and V. G. Maurino, *Mol. Plant*, 2014, **7**, 1191–1210.
74 Y. G. Sheptovitsky and G. W. Brudvig, *Biochemistry*, 1998, **37**, 5052–5059.
75 J. Ouyang, L. Wang, W. Chen, K. Zeng, Y. Han, Y. Xu, Q. Xu, L. Deng and Y.-N. Liu, *Chem. Commun.*, 2018, **54**, 3468–3471.
76 Q. Kong, Z. Zhu, Q. Xu, F. Yu, Q. Wang, Z. Gu, K. Xia, D. Jiang and H. Kong, *Small Methods*, 2024, **8**, 2301143.
77 Z. Feng, Y. Li, S. Chen, J. Li, T. Wu, Y. Ying, J. Zheng, Y. Zhang, J. Zhang, X. Fan, X. Yu, D. Zhang, B. Z. Tang and J. Qian, *Nat. Commun.*, 2023, **14**, 5017.
78 Z. Li, P.-Z. Liang, L. Xu, X.-X. Zhang, K. Li, Q. Wu, X.-F. Lou, T.-B. Ren, L. Yuan and X.-B. Zhang, *Nat. Commun.*, 2023, **14**, 1843.

Open Access Article. Published on 08 July 2025. Downloaded on 1/21/2026 5:41:23 PM. This article is licensed under a Creative Commons Attribution-NonCommercial 3.0 Unported Licence.

79 Y. Liu, H.-R. Kim and A. A. Heikal, *J. Phys. Chem. B*, 2006, **110**, 24138–24146.
80 A. A. Pakhomov and V. I. Martynov, *Chem. Biol.*, 2008, **15**, 755–764.
81 J. Kong, Y. Wang, W. Qi, M. Huang, R. Su and Z. He, *Adv. Colloid Interface Sci.*, 2020, **285**, 102286.
82 E. A. Dolgopolova, D. E. Williams, A. B. Greytak, A. M. Rice, M. D. Smith, J. A. Krause and N. B. Shustova, *Angew. Chem., Int. Ed.*, 2015, **54**, 13639–13643.
83 E. A. Dolgopolova, T. M. Moore, W. B. Fellows, M. D. Smith and N. B. Shustova, *Dalton Trans.*, 2016, **45**, 9884–9891.
84 C. R. Martin, P. Kittikhunnatham, G. A. Leith, A. A. Berseneva, K. C. Park, A. B. Greytak and N. B. Shustova, *Nano Res.*, 2021, **14**, 338–354.
85 Y. Zheng, Y. Li, C. Ke, M. Duan, L. Zhu, X. Zhou, M. Yang, Z.-X. Jiang and S. Chen, *J. Mater. Chem. B*, 2024, **12**, 2373–2383.
86 R. H. Douglas, J. C. Partridge, K. Dulai, D. Hunt, C. W. Mullineaux, A. Y. Tauber and P. H. Hynninen, *Nature*, 1998, **393**, 423–424.
87 J. Gemen, J. R. Church, T. P. Ruoko, N. Durandin, M. J. Bialek, M. Weissenfels, M. Feller, M. Kazes, M. Odaybat, V. A. Borin, R. Kalepu, Y. Diskin-Posner, D. Oron, M. J. Fuchter, A. Priimagi, I. Schapiro and R. Klajn, *Science*, 2023, **381**, 1357–1363.
88 A. A. Beharry, O. Sadovski and G. A. Woolley, *J. Am. Chem. Soc.*, 2011, **133**, 19684–19687.
89 L. J. Baker, L. L. Freed, C. G. Easson, J. V. Lopez, D. Fenolio, T. T. Sutton, S. V. Nyholm and T. A. Hendry, *eLife*, 2019, **8**, e47606.
90 J. C. Ast and P. V. Dunlap, *Environ. Microbiol.*, 2005, **7**, 1641–1654.
91 R. Tinikul and P. Chaiyen, in *Bioluminescence: Fundamentals and Applications in Biotechnology*, ed. G. Thouand and R. Marks, Springer International Publishing, Cham, 2016, vol. 3, pp. 47–74, DOI: **10.1007/10_2014_281**.
92 S. Mallidi, S. Anbil, A. L. Bulin, G. Obaid, M. Ichikawa and T. Hasan, *Theranostics*, 2016, **6**, 2458–2487.
93 N. Shah, J. Squire, M. Guirguis, D. Saha, K. Hoyt, K. K. Wang, V. Agarwal and G. Obaid, *Cancers*, 2022, **14**, 2004.
94 Y. R. Kim, S. Kim, J. W. Choi, S. Y. Choi, S.-H. Lee, H. Kim, S. K. Hahn, G. Y. Koh and S. H. Yun, *Theranostics*, 2015, **5**, 805–817.
95 X. Xu, H. An, D. Zhang, H. Tao, Y. Dou, X. Li, J. Huang and J. Zhang, *Sci. Adv.*, 2019, **5**, eaat2953.
96 Y. Yang, W. Hou, S. Liu, K. Sun, M. Li and C. Wu, *Biomacromolecules*, 2018, **19**, 201–208.
97 M.-K. So, C. Xu, A. M. Loening, S. S. Gambhir and J. Rao, *Nat. Biotechnol.*, 2006, **24**, 339–343.
98 J. Du, C. Yu, D. Pan, J. Li, W. Chen, M. Yan, T. Segura and Y. Lu, *J. Am. Chem. Soc.*, 2010, **132**, 12780–12781.
99 K. Yang, C. Wang, X. Wei, S. Ding, C. Liu, F. Tian and F. Li, *Bioconjugate Chem.*, 2020, **31**, 595–604.
100 T.-C. Chen, L. Huang, C.-C. Liu, P.-J. Chao and F.-H. Lin, *Process Biochem.*, 2012, **47**, 1903–1908.
101 N. T. Blum, Y. Zhang, J. Qu, J. Lin and P. Huang, *Front. Bioeng. Biotechnol.*, 2020, **8**, 594491.
102 C. Song, D. Huang, C. Zhao and Y. Zhao, *Adv. Sci.*, 2022, **9**, 2202829.
103 J. Hu, X. Li, L. Yang and H. Li, *Biomed. Pharmacother.*, 2022, **151**, 113068.
104 S. H. Saunders, E. C. M. Tse, M. D. Yates, F. J. Otero, S. A. Trammell, E. D. A. Stemp, J. K. Barton, L. M. Tender and D. K. Newman, *Cell*, 2020, **182**, 919–932.
105 X. Li, L. Chen, M. Huang, S. Zeng, J. Zheng, S. Peng, Y. Wang, H. Cheng and S. Li, *Asian J. Pharm. Sci.*, 2023, **18**, 100775.
106 C. Qian, P. Feng, J. Yu, Y. Chen, Q. Hu, W. Sun, X. Xiao, X. Hu, A. Bellotti, Q.-D. Shen and Z. Gu, *Angew. Chem., Int. Ed.*, 2017, **56**, 2588–2593.
107 R. M. Ryan, J. Green and C. E. Lewis, *BioEssays*, 2006, **28**, 84–94.
108 T. A. Oelschlaeger, *Bioengineered*, 2010, **1**, 146–147.
109 Y. Matsumura and H. Maeda, *Cancer Res.*, 1986, **46**, 6387–6392.
110 G. A. Swan, *Ann. N. Y. Acad. Sci.*, 1963, **100**, 1005–1019.
111 G. A. Swan and A. Waggott, *J. Chem. Soc. C*, 1970, 1409–1418, DOI: **10.1039/J39700001409**.
112 H. Lee, S. M. Dellatore, W. M. Miller and P. B. Messersmith, *Science*, 2007, **318**, 426–430.
113 I. Zmerli, J.-P. Michel and A. Makky, *J. Mater. Chem. B*, 2020, **8**, 4489–4504.
114 I. Zmerli, J.-P. Michel and A. Makky, *Multifunct. Mater.*, 2021, **4**, 022001.
115 H. Q. Tran, R. Batul, M. Bhave and A. Yu, *Biotechnol. J.*, 2019, **14**, 1900080.
116 H. Liu, Y. Yang, Y. Liu, J. Pan, J. Wang, F. Man, W. Zhang and G. Liu, *Adv. Sci.*, 2020, **7**, 1903129.
117 W. Cheng, X. Zeng, H. Chen, Z. Li, W. Zeng, L. Mei and Y. Zhao, *ACS Nano*, 2019, **13**, 8537–8565.
118 R. Prasad, V. G. S. Jyothi, N. Kommineni, R. T. Bulusu, B. B. Mendes, J. F. Lovell and J. Conde, *Nano Lett.*, 2024, **24**, 8217–8231.
119 F. Foglietta, A. Bozza, C. Ferraris, L. Cangemi, V. Bordano, L. Serpe, K. Martina, L. Lazzarato, S. Pizzimenti, M. Grattarola, M. A. Cucci, C. Dianzani and L. Battaglia, *Pharmaceutics*, 2023, **15**, 1358.
120 S. Prajapati, T. Hinchliffe, V. Roy, N. Shah, C. N. Jones and G. Obaid, *Pharmaceutics*, 2021, **13**, 786.
121 F. U. Hartl, A. Bracher and M. Hayer-Hartl, *Nature*, 2011, **475**, 324–332.
122 P. J. Muchowski and J. L. Wacker, *Nat. Rev. Neurosci.*, 2005, **6**, 11–22.
123 X. Wang, W. Zhang, L. Hou, W. Geng, J. Wang, Y. Kong, C. Liu, X. Zeng and D. Kong, *Adv. Healthcare Mater.*, 2024, **13**, 2303278.
124 M. B. Quaye and G. Obaid, *Curr. Opin. Chem. Biol.*, 2024, **81**, 102497.
125 H. S. Han and K. Y. Choi, *Biomedicines*, 2021, **9**, 305.
126 S. Bano, G. Obaid, J. W. R. Swain, M. Yamada, B. W. Pogue, K. Wang and T. Hasan, *J. Clin. Med.*, 2020, **9**, 2390.

 This journal is © The Royal Society of Chemistry 2025

Open Access Article. Published on 08 July 2025. Downloaded on 1/21/2026 5:41:23 PM.
This article is licensed under a Creative Commons Attribution-NonCommercial 3.0 Unported Licence.

127 B. Wang, L. Zhou, Y. Guo, H. Guo, Y. Zhong, X. Huang, Y. Ge, Q. Wang, X. Chu, Y. Jin, K. Lan, M. Yang and J. Qu, *Bioact. Mater.*, 2022, **12**, 314–326.
128 S. V. Shestakov and E. A. Karbysheva, *Biol. Bull. Rev.*, 2017, **7**, 259–272.
129 F. Qi, P. Ji, Z. Chen, L. Wang, H. Yao, M. Huo and J. Shi, *Small*, 2021, **17**, 2102113.
130 Z. Shen, Q. Ma, X. Zhou, G. Zhang, G. Hao, Y. Sun and J. Cao, *NPG Asia Mater.*, 2021, **13**, 39.
131 J. Yang, W. Li, L. Luo, M. Jiang, C. Zhu, B. Qin, H. Yin, X. Yuan, X. Yin, J. Zhang, Z. Luo, Y. Du and J. You, *Biomaterials*, 2018, **182**, 145–156.
132 S. Pröll, B. Wilhelm, B. Robert and H. Scheer, *Biochim. Biophys. Acta, Bioenerg.*, 2006, **1757**, 750–763.
133 P. Delcanale, C. Montali, B. Rodríguez-Amigo, S. Abbruzzetti, S. Bruno, P. Bianchini, A. Diaspro, M. Agut, S. Nonell and C. Viappiani, *J. Agric. Food Chem.*, 2016, **64**, 8633–8639.
134 T. Yamada, M. Funamoto, R. Takada, Y. Morita and T. Komatsu, *ChemBioChem*, 2024, **25**, e202400329.
135 A.-L. Bulin, M. Broekgaarden, D. Simeone and T. Hasan, *Oncotarget*, 2019, **10**, 2625–2643.
136 X. Ma, X. Liang, M. Yao, Y. Gao, Q. Luo, X. Li, Y. Yu, Y. Sun, M. H. Y. Cheng, J. Chen, G. Zheng, J. Shi and F. Wang, *Nat. Commun.*, 2023, **14**, 6187.
137 D. Satyabola, A. Prasad, H. Yan and X. Zhou, *ACS Appl. Opt. Mater.*, 2025, **3**, 552–568.
138 L. Shen, P. Wang and Y. Ke, *Adv. Healthcare Mater.*, 2021, **10**, 2002205.
139 S. Jiang, Z. Ge, S. Mou, H. Yan and C. Fan, *Chem*, 2021, **7**, 1156–1179.
140 X. Zhuang, X. Ma, X. Xue, Q. Jiang, L. Song, L. Dai, C. Zhang, S. Jin, K. Yang, B. Ding, P. C. Wang and X.-J. Liang, *ACS Nano*, 2016, **10**, 3486–3495.
141 L. Song, Q. Jiang, J. Liu, N. Li, Q. Liu, L. Dai, Y. Gao, W. Liu, D. Liu and B. Ding, *Nanoscale*, 2017, **9**, 7750–7754.
142 Q. Jiang, Y. Shi, Q. Zhang, N. Li, P. Zhan, L. Song, L. Dai, J. Tian, Y. Du, Z. Cheng and B. Ding, *Small*, 2015, **11**, 5134–5141.
143 Y. Du, Q. Jiang, N. Beziere, L. Song, Q. Zhang, D. Peng, C. Chi, X. Yang, H. Guo, G. Diot, V. Ntziachristos, B. Ding and J. Tian, *Adv. Mater.*, 2016, **28**, 10000–10007.
144 C. Walsh, M. A. Rajora, L. Ding, S. Nakamura, H. Endisha, J. Rockel, J. Chen, M. Kapoor and G. Zheng, *Chem. Biomed. Imaging*, 2023, **1**, 66–80.
145 G. Zheng, J. Chen, K. Stefflova, M. Jarvi, H. Li and B. C. Wilson, *Proc. Natl. Acad. Sci. U. S. A.*, 2007, **104**, 8989–8994.
146 T. W. Liu, M. K. Akens, J. Chen, L. Wise-Milestone, B. C. Wilson and G. Zheng, *Bioconjugate Chem.*, 2011, **22**, 1021–1030.
147 Q. Zhan, X. Shi, J. Zhou, L. Zhou and S. Wei, *Small*, 2019, **15**, 1803926.